Nanofluidic crystals: nanofluidics in a close-packed nanoparticle array

HHS Public Access

Author manuscript

Lab Chip. Author manuscript; available in PMC 2018 September 12.

Published in final edited form as:

Lab Chip. 2017 September 12; 17(18): 3006–3025. doi:10.1039/c7lc00588a.

Nanofluidic Crystals: Nanofluidics in a Close-Packed Nanoparticle Array

Wei Ouyang[1,2], **Jongyoon Han**[1,3,*], and **Wei Wang**[2,4,*]

[1]Department of Electrical Engineering and Computer Science, Massachusetts Institute of Technology, Cambridge, Massachusetts, 02139, United States

[2]Institute of Microelectronics, Peking University, Beijing, 100871, P.R. China

[3]Department of Biological Engineering, Massachusetts Institute of Technology, Cambridge, Massachusetts, 02139, United States

[4]National Key Laboratory of Science and Technology on Micro/Nano Fabrication, Beijing, 100871, P.R. China

Abstract

With various promising applications demonstrated, nanofluidics has been of broad research interest in the past decade. As nanofluidics matures from proof of concept towards practical applications, it faces two major barriers: expensive nanofabrication and ultra-low throughput. Up to date, the only material that enables nanofabrication-free, high-throughput, yet precisely controllable nanofluidic systems is the close-packed nanoparticle array, i.e. nanofluidic crystal. Recently, significant progresses in nanofluidics have been made using nanofluidic crystal, including high-current ionic diodes, high-power energy harvesters, efficient biomolecular separation, and facile biosensors. Nanofluidic crystal is seen as a key to applying nanofluidic concepts into real–world applications. In this review, we introduce the key concepts and models in nanofluidic crystal, summarize the fabrication methods, and discuss in-depth the various applications of nanofluidic crystal, highlighting its advantages in simple fabrication, low cost, flexibility, and high throughput. Finally, we provide our prospects on the future of nanofluidic crystal and its potential impacts.

TOC Image

Nanofluidic crystal bridges nanofluidics concepts with real-world applications in various fields.

*Correspondence: J. Han, jyhan@mit.edu; W. Wang, w.wang@pku.edu.cn.

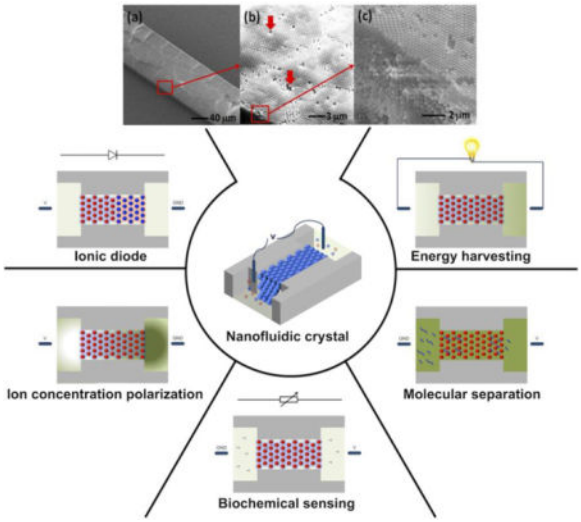

1. Introduction

As a natural extension of microfluidics and nanotechnology, nanofluidics has attracted much attention and imagination from many researchers.[1–7] Nanofluidics is defined as the study and application of fluid flow and molecular transport phenomena at nanoscale. More than a simple geometrical scaling-down from microfluidics, nanofluidic systems often involve unique and rich physical and chemical phenomena, which are often fundamental to membrane science. With the feature sizes of devices scaled down to the interaction ranges of various surface/interface forces, surface properties play an increasingly important role in the fluid and molecular transport behaviors inside nanometer-sized structures. This has been utilized to develop a large variety of novel ionic devices,[8–10] sensitive biochemical sensors,[11–13] efficient energy harvesters,[14–17] and other devices.[18–22] Although various nanofabrication approaches have been established to fabricate nanofluidic devices with precisely controlled feature sizes and functions,[23] a process as simple and cost-effective as the PDMS-based soft lithography in microfluidics is still highly desirable in the development of nanofluidic devices. Moreover, it remains a challenge to effectively and uniformly tailor the inner surface properties of nanochannels for specific applications, which is especially important in biochemical sensing.[24] The last but not the least barrier in the advancement of nanofluidics is the device throughput (functional cross-sectional area). Going beyond the proof-of-concept of nanofluidic devices, nanofluidics research has been transitioning towards practical, real-world applications. In many applications, such as energy harvesters and ionic diodes, increased throughput (at least to the level of conventional filters and membranes) is necessary, which apparently cannot be met easily by traditional nanochannel-based nanofluidics.

To overcome the aforementioned barriers in nanofluidics studies, researchers have proposed a promising nanofluidic material named nanofluidic crystal, which is a close-packed nanoparticle array (Figure 1). Monodisperse nanoparticles can spontaneously organize themselves (self-assembly) into close-packed crystalline structures under appropriate conditions.[25] The close-packed nanoparticle array, with building blocks approximately one

thousand times larger than traditional molecule crystals, has long been studied in a variety of areas, such as photonics,[26] sensors,[27] and materials.[28] However, the properties of close-packed nanoparticle array as a nanofluidic material were not realized until Zheng *et al.*[29] and Zeng *et al.*[30] utilized it for biochemical molecular separation. Since then, researchers have developed nanofluidic electrokinetic models for self-assembled nanoparticle array and exploited it for a variety of nanofluidic applications. Instead of focusing on the solid frame of the crystalline structure, one can treat the interstices of close-packed nanoparticles as a large inter-connected network of nanochannels. The highly ordered network of nanochannels is expected to possess the similar unique properties of individual nanochannels. This concept is practically important because it offers a nanolithography-free, rapid and cost-effective method of fabricating sub-100/10 nm nanochannels, the ease and flexibility of controlling surface properties, the possibility of modeling due to its ordered structure, and more importantly, presents a large functional cross-sectional area for high-throughput output as a bulk nanofluidic material (*e.g.* membranes). Like the term “photonic crystal” in photonic applications, close-packed nanoparticle array is named as “nanofluidic crystal” in nanofluidics.

While there are a number of review articles on nanofluidics,[3, 4, 31] the field of nanofluidic crystal has not been systematically reviewed. In this paper, we will summarize the up-to-date studies on nanofluidic crystal, from theory, fabrication to applications. Given that the fundamentals of conventional nanofluidics (introduced in previous review articles) can be naturally transformed to nanofluidic crystal, we will only cover concepts and knowledge essential for understanding nanofluidic crystal and those unique to nanofluidic crystal. The review is structured as follows: the second section introduces the key concepts in nanofluidic crystal; the third section introduces the fabrication methods of nanofluidic crystal; the fourth section discusses the various applications of nanofluidic crystal; finally, we will present our outlooks of nanofluidic crystal. In the text, unless otherwise specified, we will use the generalized term “nanochannel” to refer to various nanofluidic devices with different shapes, such as rectangular nanochannels, conical nanochannels, nanopores, nano-slits, and so on.

2. Fundamentals of nanofluidic crystal

2.1 Key concepts in nanofluidics

When a solid material comes into contact with an electrolyte solution, it often acquires electric charges by dissociation of surface groups and/or adsorption of ions in solution to the surface.[31] For silica surfaces, the surface charge density is typically in the range of 10–100 mC/m^2, which corresponds to one electric charge per 16–1.6 nm^2.[33] The surface charge of the solid is balanced by a layer of counter-ions in the electrolyte solution, which is denoted as the electric double layer (EDL). In the EDL, counter-ions are electrostatically attracted to the charged surface while co-ions are repelled, forming an ion concentration profile deviating from the electroneutral bulk values. The structure of the EDL is described by the Gouy-Chapman-Stern model, which is reviewed in details by Schoch *et al.*[31] The thickness of the EDL is characterized by the Debye length, which is defined as,

$$\lambda_D = \sqrt{\frac{\varepsilon_0 \varepsilon_r RT}{F^2 \sum_i z_i^2 c_i^\infty}}, \quad (2.1)$$

where ε_0 is the permittivity of vacuum, ε_r is the relative permittivity of the electrolyte, R is the gas constant, T is the absolute temperature, F is the Faraday constant, z_i is the valence of ion species i, and c_i^∞ is the concentration of ion species i in the bulk solution. The Debye length is inversely proportional to the square root of the bulk concentration. Therefore, at high ion concentrations, the EDL is thin and has negligible effects on the ion transport behaviors of nanochannels. Conversely, at low ion concentrations, the thickness of the EDL increases, leading to the counter-ion selectivity of nanochannels.

In nanofluidics, the electrical conductance is a key parameter for various applications. The bulk electrical conductance of a 1:1 electrolyte in a rectangular channel is given by the Ohm's Law, which is

$$G_{\text{bulk}} = (\mu_+ + \mu_-)\, zFc^\infty \frac{wh}{l}, \quad (2.2)$$

where μ_+ is the electrical mobility of the cation, μ_- is the electrical mobility of the anion, z is the valence of the ions, c^∞ is the concentration of ions in the bulk solution, w, h, l are the width, height, and length of the channel ($w > h$).

Because the ions in the EDL must balance the surface charge to meet the requirement of overall electroneutrality, the effective concentration of counter-ions in the EDL in a rectangular channel is given by,

$$c_e = \frac{2\,|\sigma_s|}{\mathrm{zFh}} \quad (2.3)$$

where σ_s is the surface charge density of the nanochannel. Assuming negatively charged surfaces, substituting equation (2.3) into (2.2) gives the conductance contributed by the surface charge, which is

$$G_{\text{surface}} = \mu_+ \,|\sigma_s|\, \frac{2w}{l}. \quad (2.4)$$

Therefore, the simplified expression of the total conductance of a rectangular channel with negatively charged surfaces is,

$$G = G_{\text{bulk}} + G_{\text{surface}} = (\mu_+ + \mu_-)\, zFc^\infty \frac{wh}{l} + \mu_+ \,|\sigma_s|\, \frac{2w}{l}. \quad (2.5)$$

The Dukhin number, *Du*, defined as the ratio of the surface conductance to the bulk conductance (assuming $\mu_+ \approx \mu_-$), is expressed as

$$Du = \frac{G_{\text{surface}}}{G_{\text{bulk}}} = \frac{|\sigma_s|}{zFc^{\infty}h} = \frac{l_D}{h}, \quad (2.6)$$

where l_D, the Dukhin length, is defined as,

$$l_D = \frac{|\sigma_s|}{zFc^{\infty}}. \quad (2.7)$$

When $Du >> 1$, i.e. $l_D >> h$, the conductance of a nanochannel is governed by the surface conductance, which is proportional to the surface charge density and independent of the bulk concentration. On the other hand, when $Du << 1$, i.e. $l_D << h$, the conductance of a nanochannel is proportional to the bulk concentration and independent of the surface charge density. Therefore, a surface-charged nanochannel exhibits a conductance plateau at low ion concentrations, while possessing a conductance linear with the ion concentration at high ion concentrations. This relationship is the key ion transport property in nanofluidics.

The values of the Debye length and the Dukhin length in KCl solutions with different concentrations are compared in Figure 2. It is worth noting that the Debye length is independent of the surface charge density, while the Dukhin length can be tuned by adjusting both the ion concentration and surface charge density.

2.2 Governing equations in nanofluidics

The motion of fluid and charged particles in nanochannels are governed by the Navier-Stokes, Nernst-Planck, and Poisson equations.[34–36]

First, the Navier-Stokes equation describes the motion of incompressible fluid,

$$\rho\left(\frac{\partial \boldsymbol{U}}{\partial t} + (\boldsymbol{U}\cdot\nabla)\,\boldsymbol{U}\right) = -\nabla P + \eta\nabla\cdot\nabla\boldsymbol{U} - \rho_e\nabla\varphi, \quad (2.8)$$

$$\nabla\cdot\boldsymbol{U} = 0. \quad (2.9)$$

Because of the ultra-small geometric sizes, nanofluidic devices often have an extremely large flow resistance, which makes it challenging to implement the pressure-driven flow commonly used in microfluidics.[37] Therefore, except for some cases with high driving electric fields, where electroosmosis cannot be neglected, fluid flow inside nanochannels is often negligible.

Second, the Nernst-Planck equation describes the motion of ions and charged particles,

$$\boldsymbol{J}_i = -\left(D_i \nabla c_i + z_i c_i D_i \frac{F}{RT} \nabla \varphi\right) + \boldsymbol{U} c_i, \quad (2.10)$$

$$\frac{\partial c_i}{\partial t} = -\nabla \cdot \boldsymbol{J}_i. \quad (2.11)$$

Third, the Poisson equation relates the ion concentrations to the electrical potential,

$$\nabla^2 \varphi = -\frac{\rho_e}{\varepsilon_0 \varepsilon_r}, \quad (2.12)$$

where $\boldsymbol{U}$ is the velocity, P is the pressure, ρ is the mass density, φ is electrical potential, z_i, D_i, c_i, $\boldsymbol{J_i}$ are the valence, diffusivity, concentration, and flux density of ion species I, $\rho_e = F\sum_i z_i c_i$ is the net charge density. The Nernst-Planck-Poisson equations are the basic equations in nanofluidics, and can be solved by various approaches, including commercialized finite element simulation.

2.3 Geometric model of nanofluidic crystal

In nanofluidic crystal, nanoparticles assemble into an organized structure, with the interstitial space filled with electrolyte. Hard spheres can form two types of close-packed crystalline structures, the face-centered cubic (fcc) and hexagonal close-packed (hcp). It was theoretically predicted and experimentally validated that fcc is more favored than hcp due to higher thermodynamic stability.[26, 38] A geometric model has been established to predict the ion conductance of nanofluidic crystal. As shown in Figure 3, there are two kinds of interstices in a fcc structure, tetrahedron (green) and octahedron (red). Looking at the interstice structure, one could find that each tetrahedron center is connected to four octahedron centers, while each octahedron center is connected to eight tetrahedron centers. Taking each interstitial center as a node and each connection between interstitial centers as a nanochannel, one could find that there is only one type of nanochannel in the crystalline structure, which is 1/4 tetrahedron interstitial plus 1/8 octahedron interstitial. By basic geometric analysis, the volume of the unit nanochannel is $0.023d^3$, and the total surface area of the unit nanochannel is $0.39d^2$, where d is the diameter of the nanoparticle. Since the surface-volume-ratio determines the ratio of surface and bulk conductance (Du), this interstitial nanochannel can be approximated by a cylindrical nanochannel with the same volume and surface area, which is calculated to have a diameter of $0.237d$ and a length of $0.525d$. Deriving the geometry of the unit nanochannel enables researchers to rapidly assess the optimal nanoparticle sizes of nanofluidic crystals required in specific applications. Furthermore, the electrical resistance of nanofluidic crystal can be related to the electrical resistance of the unit nanochannel by geometrical analysis of the crystalline structure.[32] It was revealed that, for a microchannel with a width of W, a height of H, and a length of L

packed with nanoparticles with a diameter of d, when an electrical field is applied along the length, its electrical resistance is,

$$R=1.414\frac{L}{WH}\cdot d\cdot R_{\text{unit}} \quad (2.13)$$

which is proportional to the diameter of the nanoparticle and the resistance of the unit nanochannel R_{unit}. The conductance of the unit cylindrical nanochannel, with a diameter of $0.237d$ and a length of $0.525d$, can be written as,

$$G_{\text{unit}}=R_{\text{unit}}^{-1}=0.086\left(\mu_{+}+\mu_{-}\right)zFc^{\infty}d+0.46\mu_{+}\left|\sigma_{s}\right| \quad (2.14)$$

Therefore, as with single nanochannels, the conductance of nanofluidic crystal exhibits a plateau at low ion concentrations, and is proportional to the ion concentration at high ion concentrations (Figure 4).

2.4 Nanoparticle doping model

The resemblance between electrolytes and semiconductors has been pointed out for a long time.[39–41] The electrons and holes in semiconductors are similar to the hydrogen ions and hydroxyl ions in water. The flow of ions and electrons are both driven by diffusion and migration. Ions in dilute electrolytes and non-degenerate electrons both obey the Maxwell-Boltzmann statistics. The positively and negatively charged surfaces of nanochannels play similar roles as the donors and acceptors in semiconductors. Despite the similarities, there are also differences between electrolytes and semiconductors. The ions of strong electrolytes, such as KCl, do not recombine as the electrons and holes do in semiconductors. The diffusivities (and more importantly, electrical mobility) of ions in water are much smaller than those of electrons and holes in semiconductors. Detailed comparison of electrolytes and semiconductors can be found in the doctoral dissertation of Li-Jing Cheng.[42]

Here we introduce a ‘doping’ model of nanofluidic crystal. Although still in its infancy, this model can potentially enable researchers to design nanofluidic devices with well-established semiconductor theories and softwares.[43] An electrically neutral nanoparticle function as an ‘intrinsic’ semiconductor atom, while a positively (negatively) charged nanoparticle serve as an ionized donor (acceptor). The degree of doping is determined by the space occupancy rate and surface charge density of the nanoparticles (Figure 5(a)). Charges of the nanoparticle ‘dopants’ are treated as uniformly distributed, which leads to the doping density of a unit cell in an fcc structure with only uncharged nanoparticles and charged nanoparticles with the same surface charge density,

$$N_{\text{doping}}=-\frac{\sum_{i}m_{i}\rho_{i}}{qV_{\text{cell}}}=-\frac{\pi\alpha\sigma_{s}}{\sqrt{2}qR} \quad (2.15)$$

where m_i, ρ_i, q, V_{cell}, α, σ_s, R are the number of nanoparticle species i, the charge of nanoparticle species i, charge of an electron, the volume of a unit cell, the ratio of the charged nanoparticles, the surface charge density of the charged nanoparticles, and the radius of the nanoparticles.

Neglecting fluid flow, the governing equations of an electrolyte doped with nanoparticles are similar to semiconductors, which are,

$$\boldsymbol{J_k} = -z_k q \eta_k^* \nabla \phi_i - z_k q D_k^* \nabla n_k, \quad (2.16)$$

$$\frac{\partial n_k}{\partial t} = -\frac{1}{z_k q} \nabla \cdot \boldsymbol{J_k} - R_k + G_k, \quad (2.17)$$

$$\nabla^2 \phi_i = \frac{-q(-N_{\text{doping}} + \sum_k z_k n_k)}{\varepsilon_0 \varepsilon_r}, \quad (2.18)$$

where J_k, z_k, η_k^*, D_k^*, n_k, R_k, G_k, ϕ_i, t are the electrical current density, valence, effective mobility, effective diffusivity, ion density, recombination rate, generation rate of ion species k, electrical potential, and time.

With the doping model, nanofluidic crystal devices can be analyzed by adopting the equations from semiconductor physics. For example, the electrical current density of a nanofluidic crystal diode under a bias is similar to that of a semiconductor diode, which is

$$J_1 = \left(\frac{D_n^* n_i^2 q}{L_n N_a} + \frac{D_p^* n_i^2 q}{L_p N_d} \right) \left(e^{qV/k_B T} - 1 \right), \quad (2.19)$$

$$L_n = \sqrt{D_n^* \tau_n}, \qquad L_p = \sqrt{D_p^* \tau_p}, \quad (2.20)$$

$$\tau_n = \frac{1}{k_{H^+,\, OH^-} N_a}, \ \tau_p = \frac{1}{k_{H^+,\, OH^-} N_d}, \quad (2.21)$$

where V is the electrical bias, and $k_{H^+,\, OH^-}$ is the reverse reaction rate of water ionization. This model has been used to predict the current rectification behaviors of nanofluidic crystal diodes with oppositely charged nanoparticles. Figure 5(b) shows simulated electrostatic potential, electrochemical potential for hydrogen, and hydroxyl ions in a nanofluidic crystal

diode. Simulated and experimental I-V curves of nanofluidic crystal diodes are shown in Figure 5(c).

3. Fabrication of nanofluidic crystal

Self-assembly of colloidal particles is an intensively studied subject in chemistry and material science, and the field of photonic crystal boosted the development of techniques that enable the constructions of intricate crystalline structures.[44] Generally speaking, the self-assembly of nanoparticles can be controlled by confinement on patterned substrates, manipulated by interfacial forces (e.g. capillary force, surfactant-assisted assembly, assembly in nematic liquid crystal and emulsions), guided by external fields (e.g. light, electric field, magnetic field), and directed by linking surface functional groups.[25, 44–47] For the fabrication of nanofluidic crystal, researchers mainly adopt capillary force-assisted assembly of nanoparticles, which can be categorized into two methods: vertical deposition[29, 48–59] and horizontal deposition.[60–64] Figure 6(a) shows the scheme of vertical deposition.[65, 66] In this method, a solid substrate is placed vertically in a nanoparticle suspension. The evaporation of solvent causes the meniscus to swipe across the substrate vertically downward. During this process, nanoparticles are transferred from the bulk to the drying front by a convective flow and assemble at the drying front in a well-ordered manner. This method may allow the formation of large-area crack-free crystals under a controlled evaporation rate and in a vibration-free environment.[66] Moreover, the thickness (number of layers) of the assembled crystal can be precisely controlled by the concentration of nanoparticles in the suspension. However, as the nanoparticles are assembled in an open environment in vertical deposition, it is not straightforward to define the morphology of the assembled crystal as desired. Additionally, in many micro/nanofluidic applications, it is necessary to confine the assembled crystal in enclosed channels. This may be realized by mounting a PDMS channel on top of the crystal,[29] but matching the dimensions of the PDMS channel and the crystal could be technically difficult.

In contrast, the horizontal deposition method enables *in situ* assembly of nanoparticles in pre-defined micro/nano structures. Figure 6(b–e) illustrate the process of horizontal deposition. To assemble nanoparticles in a single microchannel, a droplet of nanoparticle suspension is first loaded into one reservoir. The nanoparticle suspension propagates along the microchannel by capillary force, and stops at the opposite end of the microchannel because an additional pressure is required for it to counter the effect of surface tension and pass the geometrical expansion. The detailed conditions for the self-limiting effect was derived by Choi *et al.*[62, 63] After the nanoparticle suspension stops, the reservoir loaded with the nanoparticle suspension is covered to induce unidirectional evaporation at the opposite end of the microchannel. As solvent evaporates, additional solvent moves toward the evaporation edge to compensate the loss of solvent, bringing together nanoparticles towards the evaporation front. As evaporation continues, nanoparticles self-assemble into an ordered lattice from the evaporation front to the other end of the microchannel (Figure 6(b)). The self-assembly process can be stopped by replacing the nanoparticle suspension with solvent. The assembled nanoparticle array is typically naturally dried at room temperature or elevated temperatures to stabilize the crystalline structure, after which it can withstand high electric fields.[30] Following a similar process, nanoparticles can also be assembled in a

micropore to form a thin membrane (Figure 6(c)), which have been used for salt-gradient energy harvesting applications.[60] To assemble nanoparticles in a specific region of a microfluidic chip, assisting microchannels are often used at the boundaries of the designated region to deliver nanoparticles and serve as the geometrical expansion needed for the self-stopping of nanoparticle suspension (Figure 6(d)). Nanoparticle suspension is introduced through one assisting microchannel, part of which flows to the designated region and self-stops at the geometrical expansion.[61] After assembled nanoparticles have filled up the designated region, buffer is loaded to rinse the assisting microchannel. The chip will be ready for use after assembled nanoparticles in the designated region has dried up. Large-scale nanofluidic crystals are often needed in continuous-flow biomolecular separation and other applications, which is challenging to pattern due to the formation of cracks.[71] Nanoparticles patterned in large-area microchannels have cracks periodically spaced along the evaporation front and propagating in parallel from the evaporation front to the bulk, which is attributed to the heterogeneous capillary stress built across a large area during the evaporation.[71–74] Zeng *et al.* proposed multiple microchannel guided patterning of crack-free large-scale nanofluidic crystal, which reduced the stress non-uniformity by dividing the wide evaporation front to segments shorter than the length above which crack occurs.[71] Using this method, nanofluidic crystal with an area of 4×4 mm^2 was fabricated without cracks (Figure 6(e)).

Overall, we believe the fabrication techniques for nanofluidic crystal currently developed are simple, low-cost, rapid, and provide sufficiently large throughput (cross-sectional area>10 mm^2) for researches at this stage. The main issue revolving the fabrication of nanofluidic crystal is the reproducibility, which is affected by two factors, crack formation and variation in dimensions. In both vertical and horizontal depositions, cracks can be reasonably well controlled by device design and the conditions of crystal growth, such as evaporation rate, nanoparticle concentration, and avoidance of vibration.[56, 65, 71] The additions of photopolymer gels and silica precursors during crystal growth have also been reported to protect the assembled crystals from cracking.[75, 76] In terms of the crystal dimensions, horizontal deposition in pre-defined structures provides a more stringent definition than vertical deposition, which relies on controlling the concentration of nanoparticles and other conditions.[65] Nevertheless, technically, the length of microfluidic channels may vary during manual punching of reservoirs, and residual nanoparticle assembly outside of micropore is often hard to avoid, which may hamper the reproducibility in some applications.[32, 77] To gain a full control over the dimension of nanofluidic crystal, one will need to employ additional assisting microchannels for nanoparticle delivery, as shown in Figure 6(d). To sum up, we compare the features of different fabrication methods in Table 1 for readers' quick reference.

Lastly, we believe there is still a lot that the nanofluidic crystal community can learn from photonic crystals. Delicate fabrication techniques, which involve the management of particle shape and size, particle-particle interaction, interactions between particles and surroundings, have been developed for the fabrication of intricate photonic crystal devices. These techniques can help improve the quality of nanofluidic crystal and endow researchers with more freedom in the design of nanofluidic crystal devices. With better control over the assortment of nanoparticles, we can hopefully expect the further scaling-up of nanofluidic

crystal, both dimensionally and functionally, to enable nanofluidic devices with ultra-high throughput and integrated nanofluidic systems (circuits) composed of synergic functional subunits.

4. Applications

4.1 Ion transport regulation

Ion transport regulation (ITR) is an electrochemical phenomenon uniquely existing in nanochannels, because electrostatic interaction between ions and charged surfaces becomes prominent only at nanoscale. ITR has received much attention in the past decade, motivated by its potential applications in controlled molecule delivery, biomolecular detection, model studies of biological ion channels, and *etc.*[10, 78] ITR stems from the unipolar distribution of ions in the EDL near the charged surfaces of nanochannels, in which the passage the passage of counter-ions is favored over that of co-ions, i.e. ion-selectivity. Ion-selectivity enables selective transport of cations/anions between two compartments via nanochannels, but the direction of transport is fully reversible for symmetric systems by simply reversing the driving forces. What has been of more interest is, preferentially allowing ion transport in one direction while inhibiting it in the opposite direction (resembling the semiconductor diode), which is often specifically referred to as ion current rectification (ICR). The key to achieving ICR is introducing direction-dependent differential ion-selectivity in a single device, which is commonly realized by asymmetric surface charge distribution, asymmetric geometry, and asymmetric bath concentrations. A variety of nanochannel-based diodes (and even transistors) have been developed using the aforementioned three approaches. Although more recent papers have emerged,[79–83] the review paper by Cheng *et al.*[8] in year 2010 provides an in-depth tutorial of the principle and design of nanochannel-based diodes for readers' reference.

For engineering ITR systems, nanofluidic crystal is advantageous over nanochannels mainly in two aspects. First, the diameter and surface property of nanoparticles are readily tunable for the parameter optimization of nanofluidic diodes, without going through the complicated processes of nanochannel fabrication and modification. Second, compared to the limited ionic fluxes of nanochannels, nanofluidic crystal supports high-throughput yet regulated transport of ions due to its highly ordered and easy-to-scale-up features. Zharov and coworkers studied ion-selectivity in nanofluidic crystal using nanoparticles functionalized with ionizable groups and responsive polymer brushes.[50, 51, 53, 67] By voltammetric measurements, they found that the limiting current of $Ru(NH_3)_6^{3+}$ through nanofluidic crystal was reduced in aminated (positively charged) nanofluidic crystal, but increased in sulfonated (negatively charged) nanofluidic crystal, which was attributed to the electrostatic repulsion and attraction effects of positively ($-NH_3^+$) and negatively ($-SO_3^-$) charged surfaces on $Ru(NH_3)_6^{3+}$, respectively. The electrostatically induced selectivity was confirmed by the observation that in sulfonated nanofluidic crystal the limiting current of $IrCl_6^{3-}$ was reduced and that of uncharged $Fc(CH_2OH)_2$ (1,1′-Ferrocene Dimethanol) was unaltered.[53] The authors further demonstrated the modulation of ion-selectivity in sulfonated nanofluidic by adjusting the pH and ionic strength of electrolyte. It was found that with the increase of pH from acidic to basic, the limiting current of $Ru(NH_3)_6^{3+}$ increased and that of

$IrCl_6^{3-}$decreased, due to the change of the surface charge polarity from positive to negative. Meanwhile, as expected, the ion selective effect diminished as they increased ionic concentration from 50 mM to 500 mM, owing to the suppression of the EDL. More recently, the authors explored another paradigm of surface modification using responsive polymer brushes, which were shown to electrostatically and/or sterically regulate ion transport. Thus-induced ITR has so far been demonstrated with temperature-responsive poly(N-isopropylacrylamide) (PNIPAM)[52] and Polyalanine,[56] pH-responsive poly(2-(dimethylamino)ethyl methacrylate) (PDMAEMA),[55] and small molecule binding responsive aptamers.[57] For example, in PDMAEMA-filled nanofluidic crystal, the flux of $Ru(NH_3)_6^{3+}$ was shown to drop abruptly at low pHs due to the protonation (electrostatic effect) and stretching (steric effect) of polymer chains. In comparison, the neutral molecule $Fc(CH_2OH)_2$ only had a ~30% drop in limiting current, which corresponded exclusively to steric hindrance of the PDMAEMA chains.[55]

Based on similar principles, nanofluidic diodes were developed by inducing differential ion-selectivity in single nanofluidic crystal devices. Corresponding to the three distinct approaches of realizing nanochannel-based diodes, nanofluidic crystal based diodes could be realized by using nanoparticles with different surface properties, or by using nanoparticles of different diameters, or by employing bulk solutions with different ion concentrations. As shown in Figure 7, we depicted the general guidelines of optimizing the performances of different types of nanofluidic crystal based diodes using phase charts. The quantitative condition for ion-selectivity is that, at a certain ion concentration, the Dukhin length is larger than the equivalent nanochannel diameter (24% of the nanoparticle diameter), expressed as $l_D > 0.24d$, i.e. $Du > 1$. Under this condition, the surface conductance that features selective-transport of ions is dominant over the bulk conductance, thereby satisfying the selectivity of transported ions. In the ion-selective regime, the ion-selectivity increases as the EDLs transit from non-overlapping to higher degrees of overlapping. In other words, in the order-of-magnitude sense, $Du > 1$ can be treated as a necessary condition of ion-selectivity, while EDL overlapping is a sufficient condition of ion-selectivity.

For the first type of diode by packing nanoparticles with opposite charge polarities (Figure 7(a)), the differential ion-selectivity comes directly from the opposite surface charges of the nanoparticles. When the electrical potential drops from the negatively charged side to the positively charged side of the nanofluidic crystal, both cations and anions migrate towards the junction but could not cross it due to electrostatic repulsion, resulting in the accumulation of ions and a large forward current. Oppositely when the bias is reversed, both cations and anions migrate out of the junction but there are no supplement ions from the bulk due to the electrically blocked passage, resulting in the depletion of ions in the nanofluidic crystal and a small reverse current. To obtain higher rectifying factors, one can decrease the nanoparticle diameter for stronger overlapping of the EDLs, which at the same time increases the ionic current throughput due to higher concentrations of ions in the nanoparticle interstitials (Figure 7(b)). One can also increase the rectifying factor by using lower concentrations of buffers to enhance the ion-selectivity, though the ionic current throughput is correspondingly decreased (Figure 7(b)). This type of diode was first demonstrated by packing silica nanoparticles with opposite charge polarities in a double-pyramid-shaped micropore.[84] As shown in Figure 7(c), the I-V curves displayed a diode-like

behavior with a rectifying factor of 24 in a 500 nm nanofluidic crystal, which increased to 48 in a 173 nm nanofluidic crystal due to the decreased equivalent channel size and in turn strengthened ion-selectivity.

The second type of diode is formed by packing nanoparticles of different sizes (Figure 7(d)). In the small nanoparticle end, there is strong overlapping of the EDLs, thereby strong ion-selectivity. In the large nanoparticle end, the ion-selectivity is weak due to the larger equivalent channel size. Upon the application of a voltage, both the cation flux and anion flux into and out of the small nanoparticle region mismatch, resulting in the accumulation and depletion of ions in the small nanoparticle end at opposite electrical biases. The accumulation of ions corresponds to a large forward current, while the depletion of ions corresponds to a small reverse current. In Figure 7(e), each pair of points (boxed) represents the nanoparticle pair of different sizes in a diode of this type at a certain ion concentration. With the decrease of the ion concentration, the small nanoparticle end enters the strong EDL-overlapping regime, resulting in the increase of the rectifying factor. However, as the ion concentration continues to decrease, both the small and large nanoparticle ends enter the strong EDL-overlapping regime, weakening the asymmetry of ion-selectivity and in turn reducing the rectifying factor. Rao *et al.*[85] demonstrated this type of diode with free-standing nanosheets formed by two layers of differently sized Au nanoparticles (Figure 7(f)). The rectifying factor increased at lower ion concentrations, and reached its maximum at 0.1 mM in a 14.69/51.64 nm nanosheet. They also found that the rectifying effect was more significant in nanosheets with stronger size asymmetry, with a maximum rectifying factor of 13 achieved in a 14.69/76.57 nm nanosheet.

The third type of diode is realized by asymmetric bath ion concentrations at the two ends of a homogeneous nanofluidic crystal (Figure 7(g)). The principle of this type of diode is similar to that of the second one. There is strong ion-selectivity in the low bath concentration end and weak ion-selectivity in the high bath concentration end, which leads to the accumulation and depletion of ions in the low bath concentration end. In Figure 7(h), each pair of points (boxed) represents the two bath concentrations in a diode of this type at a certain nanoparticle diameter. Increasing the ion concentration of the high concentration bath enhances the asymmetry of ion-selectivity, thereby increasing the rectifying factor. However, at sufficiently high concentrations of the high concentration buffer, the ion-selectivity throughout the nanofluidic crystal diminishes, resulting in the loss of the diode characteristics. Up to date, no dedicated experimental demonstration of this type of diode has been reported. Nevertheless, an interesting variant of this diode was developed by Choi *et al.*[86] The authors first established ion-selectivity with low ion concentration buffer in a nanofluidic crystal packed in an asymmetric microchannel. It was found that, after replenishing the low ion concentration buffer with high ion concentration buffer, the ion-selectivity was still preserved in the small-opening end but diminished in the large-opening end. Based on the differential ion-selectivity, the authors achieved a maximum rectifying factor of 55 at ±10 V in an asymmetric microchannel with tip openings of 10 μm and 200 μm with nanoparticles of 240 nm in 10 mM KCl. Unlike its nanochannel-based counterparts, whose rectified ionic currents did not exceed tens of nanoamperes, this work achieved currents up to microamperes under the same conditions, benefitting from the high-throughput characteristic of nanofluidic crystal.

4.2 Ion concentration polarization (ICP)

ICP refers to the phenomenon that, as a DC voltage (typically tens to hundreds of volts) is applied along an ion selective nanochannel, ions are enriched at one end and depleted at the other end, which arises from the mismatched ionic fluxes in the bulk and ion selective nanochannel.[87] ICP devices are often designed that a tangential electroosmotic flow is concurrently induced by the DC voltage applied in the microchannel at the ion depletion side, which allows continuous processing of samples and in some applications continuous concentration of target molecules at the depletion zone boundary by as high as several million folds.[88] Benefitting from these intriguing features, ICP has been extensively studied in the past decade for a variety of applications, such as biomolecule concentration,[89] water desalination,[90] and chemical mixing.[91] However, as pointed out by Choi *et al.*,[62] the efficiency of generating ICP, which favors high ionic fluxes and low fluidic resistance in the ion-selective nanochannel, is significantly limited by the availability of materials. Currently ion-selective nanochannels are mainly made by two classes of materials, top-down fabricated nanochannels and permselective membranes (e.g. Nafion). For top-down fabricated nanochannels, besides the sophisticated processes and/or costly and specialized equipment required, the limited throughput and two-dimension restriction of current nanofabrication techniques make it challenging to increase ionic flux, and to reduce fluidic resistance. On the other hand, permselective membranes, while providing high ion throughput, lack controllability and flexibility for the improvement of the ICP generation efficiency. First, it is hard to precisely control the size, shape, and location of the membranes in microfluidic devices. Second, permselective membranes (often polymeric soft materials) are not sufficiently robust both mechanically and chemically, which may change volume upon desorption of water and gradually degrade during operation.[92] Finally, it is also challenging to tune the pore size and surface property of the membranes for optimal performances.

In recent years, nanofluidic crystal has emerged as a novel material for ICP generation, because it shares the merits of nanochannels and permselective membranes without inheriting their shortcomings. By *in situ* self-assembly of functionalized nanoparticles, nanofluidic crystal provides a three-dimensional, highly ordered, yet easy-to-scale-up nanochannel network with precisely controllable geometry and location and many degrees of freedom that can be utilized to optimize the performance of the device. The use of nanofluidic crystal as an ICP-generating material was first demonstrated in a water desalination device by Choi *et al.* in year 2012 (Figure 8(a)).[93] Instead of using Nafion, which was deployed in the pioneering work of nanofluidic desalination by Han and co-workers,[90] the authors constructed the nanojunction with a geometry-controlled nanofluidic crystal through “one-step stamping” and self-assembly. The device was shown to successfully desalt water using the ion depletion effect of ICP, though the performance of desalination was not fully characterized. It remains to be elucidated how nanofluidic crystal compares with conventionally used Nafion, or commercially available cation-exchange materials, in terms of the desalination performance. The application of nanofluidic crystal in ICP was further demonstrated in biomolecule concentration by Syed and co-workers (Figure 8(b)).[94] By using a 300 nm nanofluidic crystal as a nanojunction between two microfluidic channels, the authors were able to concentrate DNA molecules by 1700 times in 15 min and

protein molecules by 100 times in 5 min. More recently, an active micromixer was developed with nanofluidic crystal, which took advantage of the strong convection generated by the non-equilibrium electrokinetics in the ion depletion zone (Figure 8(c)).[63] Owing to the remarkably larger interacting area with the sample channel, the nanofluidic crystal-based micromixer obtained a 2-fold shorter mixing time (~0.78 ms) and a 34-fold shorter mixing length (~7.86 μm) than previous nanochannel-based devices.

Although applications of nanofluidic crystal in ICP had been showcased, the underlying electrokinetics was not clarified until the study of Choi and co-workers.[62] Choi *et al.* experimentally investigated the correlation between parameters of nanofluidic crystal and nanoscale electrokinetics, and theoretically examined the mechanisms underneath. It was found that the onset time of ICP and I-V characteristics strongly relied on the size and materials of the nanoparticles, geometry of the nanofluidic crystal and buffer conditions. As the nanoparticle size was reduced from 700 nm to 200 nm, the onset time of ICP decreased, while the ionic conductance increased, due to the promoted propagation of the depletion layer and enhanced ion concentration inside the nanofluidic crystal at smaller nanoparticle diameters. Interestingly, this trend reversed as the nanoparticle size was further reduced from 200 nm to 100 nm, which was speculated to result from the prominent steric exclusion and hydrodynamic drag or increased tortuosity at smaller scale. Moreover, as the width and height of the nanofluidic crystal increased, the onset time was shown to decrease due to enhanced electrical conductance. At the same time, the I-V curves implied the vanishing of limiting current at smaller widths of the nanofluidic crystal due to the vortex pairs that became dominant. Finally, the pH of the buffer and the materials of nanoparticles also elicited notable responses in the onset time and I–V characteristics of ICP. The electrical conductance of the nanofluidic crystal decreased as the surface charge density decreased from pH 9.4 to pH 5.6, but increased dramatically at pH 4.0 where the contribution of the hydronium ion to the conductivity won over the counteracting effect from the decrease of surface charge. Additionally, compared to the hydrophilic silica nanoparticles, the hydrophobic polystyrene nanoparticles endowed nanofluidic crystal with higher ion flux and in turn shorter onset time, owing to the amplified hydrodynamic slippage at hydrophobic surfaces. In conclusion, the phenomena observed in the nanofluidic crystals can be explained by the same theoretical principles used to explain ion transport in ion selective membranes or solid-state nanochannels, but one can find much more diverse, complicated behaviors depending on the choice of nanoparticle sizes, surface chemistry, and other controllable experimental parameters. This clearly demonstrates the power of nanofluidic crystal as a tool to investigate these multiphysics, multi-scale phenomena with much more experimental controllability.

4.3 Energy harvesting by reverse electrodialysis

Another interesting application originating from the ion-selectivity is energy harvesting from salinity gradient. Salinity gradient energy is sustainable and exists vastly in nature, considering the immerse seawater and fresh water available on the earth. When two fluidic compartments with a salinity gradient are connected by ion-selective materials, a net electrical current is generated as ions with opposite charges diffuse with unmatched rates, which is termed reverse electrodialysis (RED).[95] Although the majority of RED research is

focused on developing large-scale systems for domestic and industrial uses, there have been increasing interests in miniaturized RED devices as the need for self-powered micro/nanodevices emerges. Conventional large-scale RED systems are based on ion-exchange membranes, which present substantial challenges in the miniaturization and integration of RED systems due to their poor controllability, flexibility, and robustness as aforementioned. Alternatively, nanochannels are explored as a novel platform for micro/nano-scale RED, which have proved to generate considerably higher power densities than their ion-exchange membrane counterparts.[17, 96] Moreover, the capability of precisely defining the geometry of nanochannels may also catalyze the discovery of new mechanisms and drive further improvement of the performance of RED. However, when it comes to practical applications, nanochannel-based systems apparently face the challenge of scaling up. Micro/nanodevices usually operate at powers ranging from nanowatts to microwatts,[97] which are well beyond the maximum power currently achievable in nanochannel based RED systems (tens of picowatts). The problem of limited output power can be potentially solved by substituting nanochannels with the highly scalable and well-controlled nanofluidic crystal, without compromising the good controllability and robustness of nanochannels.

Nanofluidic crystal-based RED was first reported in year 2013.[60] Silica nanoparticles were packed in a KOH-etched 40×40 μm^2 micropore, after which the entire chip was clamped between two milliliter-scale PMMA reservoirs with different concentrations of potassium chloride (Figure 9(a)). To obtain a high open-circuit voltage (V) and output power (P), one will ideally need to maximize the concentration gradient, ionic flux and the ion-selectivity. However, increasing the ion concentration leads to the decrease of the Debye length, which trades off the ion-selectivity, reduces the energy conversion efficiency (η), and in turn could reduce V and P. The optimal conditions for maximizing the energy harvesting performance were experimentally investigated, which were summarized in Figure 9(b). In Figure 9(b), each pair of points (boxed) represents the concentration gradient of an energy harvester at a certain nanoparticle diameter. The low concentration end is set to 0.1 mM. As the high concentration increases from 0.3 mM to 100 mM, the high concentration end gradually loses ion-selectivity. As a result of the interplay between the concentration gradient and ion-selectivity, the maximum open-circuit voltage is gained at intermediate gradients, which reached 90 mV at 0.1 mM|30 mM in a 100 nm nanofluidic crystal and 20 mV at 0.1 mM|3 mM in a 500 nm nanofluidic crystal in the work of Ouyang *et al.*[60] Under the same concentration gradient, the higher open-circuit voltage of 100 nm over 500 nm nanofluidic crystal is attributed to the stronger ion-selectivity at smaller diameters. The energy conversion efficiency deceases at higher concentrations due to the weakened ion-selectivity. Despite the lower efficiency, the maximum output power is obtained at the highest concentration gradient, because the highest electrical conductance (ionic flux) outweighs the impact of the lowest energy conversion efficiency.[60] This device attained a power density (2.82 W/m^2) comparable to nanochannel-based RED systems, but the output power were amplified by more than two orders of magnitude (1.17 nW), which proved the scalability of nanofluidic crystal for meeting the power requirements of micro/nanodevices.[60] Choi *et al.* performed a more detailed parametric study of nanofluidic crystal-based RED by precisely defining the geometry of nanofluidic crystal in a microfluidic channel.[61] Besides the size of nanoparticle and ion concentrations, the authors revealed that the geometry of nanofluidic

crystal and the materials of nanoparticles also played an important role in determining the performance of RED. Increasing the height of nanofluidic crystal enhanced the ionic flux but weakened the concentration gradient, which had an overall effect of increasing the output power. Shortening the length of nanofluidic crystal increased electrical conductance, which significantly improved the output power on the condition that ion-selectivity was not overly weakened. Finally, carboxylate polystyrene nanoparticles were shown to offer higher conversion efficiency, output voltages and powers than silica nanoparticles of the same size as a compound effect of higher surface charge density and hydrodynamic slippage at the hydrophobic surfaces of nanoparticles.

4.4 Molecular separation

The need for efficient molecular separation is ubiquitous and paramount in chemistry and biology, with applications ranging from chemical processing to genomics, proteomics and molecular biology. Amongst others, gel electrophoresis (GE) and liquid chromatography (LC) are the most widely used techniques for molecular separation. The separation mechanisms differ from technique to technique: GE utilizes the different migration velocities of differently sized/charged molecules under electric field, while LC relies on the differential partitioning of analyte molecules between the mobile phase and stationary phase due to different hydrophobicity/polarity/affinity/sizes/charges. Conventionally, most separation techniques rely on gels or polymer matrices, which are inexpensive and provide molecular-scale pores with relatively high throughput.[98, 99] However, the uncontrollable pore sizes in gels or polymer matrices prevents the engineering of the materials for better performance, while the low electric field they can stand also limits the resolution and speed of separation. Micro/nanofabricated molecular sieving systems have received much interest owing to the highly regular and precisely engineered geometry, high electric field tolerance and mechanical/chemical robustness they offer. It has been demonstrated that micro/nanofabricated systems significantly improve the efficiency and speed of biomolecular separation.[100–104] The highly controllable nature of micro/nanofabricated systems also catalyzes the study of new separation mechanisms, such as entropic trapping,[105, 106] Brownian ratchets[102, 107] and hydrodynamic sorting.[104, 108] However, micro/nanofabricated systems suffer from the aforementioned issues of fabrication. For molecular separation application, nanofluidic crystal possesses the merits of both gel/polymer matrices and micro/nanofabricated systems while overcoming their drawbacks. In addition, nanofluidic crystal possesses the great flexibility in tuning the pore size and surface property to target specific ranges of molecule sizes and specific mechanisms of separation. Pore sizes can be scaled down to ~10 nm for separation of small molecules, by simply assembling nanoparticles around 100 nm, which would have been much more challenging with standard micro/nanofabrication techniques.

Nanofluidic crystal was initially used to study the electro-migration of single DNA molecules.[48, 109] It was observed that the behavior of single DNA molecules in nanofluidic crystal was comparable to that in gel/polymer matrices and micro/nanofabricated systems. Nanofluidic crystal was also shown to endure an electric field of 200 V/cm without any damage in crystal structure (likely benefitting from the strong van del Waals forces and hydrogen bonds between close-packed particles), which was considerably higher than in

conventional GE.[48] Encouraged by the promise of nanofluidic crystal as a material for molecular separation, a few groups (I. Zharov/M. J. Wirth/D. Jed Harrison) investigated nanofluidic crystal-based molecular separation for small molecules, proteins and DNAs. Zharov and co-workers demonstrated size-based separation of polyamidoamine dendrimers (2–20 nm) in nanofluidic crystal, and the tortuous paths molecules took through the nanochannel network enhanced the separation efficiency.[58] The same group further realized enantiomers separation in nanofluidic crystal modified with chiral selector moieties, achieving performance on par with most reported polymer-based solid membranes and bulk liquid membranes.[59] Wirth and co-workers[29] demonstrated high-speed chemical separations in a 200 nm nanofluidic crystal. Three cationic, hydrophobic dyes were separated based on reversed-phase adsorptivity in 6 s over an unprecedentedly short separation length of 1 mm by using a C_{18} stationary phase and a field strength of 1000 V/cm (Figure 10(a)).[29] Three peptides were separated in the same device based on electrophoretic mobility in 10 s over a 6 mm separation length, demonstrating significantly reduced dispersion (narrower peak width) as well as greatly increased mass transport compared to commercial monolithic stationary phase.[29] Wirth and co-workers later investigated electrochromatography of proteins in a 330 nm nanofluidic crystal packed in a 75 μm capillary[68], and achieved efficient protein separation. Sub-50 nm plate heights and more than one million plates were obtained in a separation length of 12 mm, which could be valuable for miniaturized separations in microchip and lab-on-a-chip devices (Figure 10(b)). The same group further improved the performance of nanofluidic crystal for protein separation by introducing slip flow in a hydrocarbon modified nanofluidic crystal, which provided enhanced flow rates and a narrower distribution of fluid velocities.[69, 70] Slip-enhanced nanofluidic crystal was shown to separate bovine serum albumin (BSA) with a zone length 15-fold narrower than the theoretical limit for Hagen-Poiseuille flow (Figure 10(c)).[69] Moreover, slip-enhanced nanofluidic crystal was able to separate a monoclonal antibody from its aggregates with a 10-fold increase in speed compared to conventional HPLC.[69] Wirth's group also developed a theoretical model for protein separation in nanofluidic crystal based on the Ogston Model and validated it experimentally, which facilitated the design of such applications.[110]

The separation of DNA in nanofluidic crystal was demonstrated for the first time in 2007 by Harrison's group, who subsequently contributed a series of interesting papers on DNA separation. Harrison and co-workers developed a facile microfluidic patterning strategy for formation of robust and three-dimensional nanofluidic crystal, with which they achieved rapid separation of DNAs and proteins of wide size ranges.[30] By adjusting pore sizes, the authors achieved separation of double stranded DNAs (dsDNAs) of 0.05–50 kbp in 330/900/1530 nm nanofluidic crystals, and separation of SDS-denatured proteins of 20–200 kDa in 160/330 nm nanofluidic crystals, with performances comparable to gel/polymer-filled and micro/nanofabricated systems (Figure 10(d)).[30] Subsequently the same group developed a multi-channel guided self-assemble method for reducing stress and obtaining large-scale crack-free nanofluidic crystals (4×4 mm^2), with which they realized high-throughput continuous-flow separation of dsDNAs of 2–50 kbp by the pulsed field separation technique (Figure 10(e)).[111] Using a similar device, Harrison and co-workers theoretically and experimentally studied the effects of electric field strength, frequency and DNA size on separation resolution, which provided insights into the design of nanofluidic

crystal-based DNA separation device for specific applications.[112] In addition to the aforementioned parameters to tune the separation resolution, Harrison's group also demonstrated that pore size gradients introduced by packing differently sized nanoparticles could also be tuned to increase the peak capacity in DNA separation.[113] Next, the same group systematically evaluated the effect of order on DNA separation resolution by doping nanofluidic crystal with differently sized nanoparticles to introduce different degrees of disorder (Figure 10(f)).[114] It was discovered that ordered structures gave large separation distances, smaller band broadening and better resolution than highly disordered structures. More interestingly, short range order offered better performance than the long range one.[114] In summary, with the various merits nanofluidic crystal owns in molecular separation, we believe nanofluidic crystal-based separation systems will continue to flourish and provide even better performance in the future, as well as scientific insights on how molecular sieving works at the nanoscale.

4.5 Biochemical sensing

Because of the important role biochemical detection plays in medicine and life sciences, there have been extensive efforts devoted to developing sensitive and specific biochemical sensing techniques. Amongst others, nanofluidic sensors have been of wide interest owing to the capability of label-free biochemical detection and the direct signal transduction from bio-reaction to electrical readout in nanochannels. Karnik *et al.*[11] first studied the effects of biomolecule binding on the conductance of nanochannels, revealing two mechanisms of nanofluidic biosensing: the volume exclusion effect in which the binding of target molecules to immobilized surface probes changes the effective cross-sectional areas of nanochannels and in turn regulates the flux of ion transport, and the electrostatic effect in which the binding of target molecules changes the surface charge densities of nanochannels and in turn regulates the concentration of ions in the channels. Based on the volume exclusion effect, Ali *et al.*[115] detected streptavidin (~3 nm) as low as 1 pM in conical nanopores with a tip opening of ~8 nm in 100 mM KCl solution. Using the electrostatic effect, Karnik *et al.*[11] and Schoch *et al.*[116] demonstrated detection of streptavidin in biotin-coated 30 nm and 50 nm deep silica nanochannels, respectively. Duan *et al.* realized detection of trypsin down to 0.2 nM in 52 nm deep nanochannels in DI water,[13] while Liu *et al.* achieved a limit of detection (LOD) of 0.3 fM for troponin T protein in conical nanochannels with a tip opening size of 70 nm in 1.6 mM phosphate buffer.[12]

Despite being label-free and highly sensitive, the practical application of nanofluidic biochemical sensing is significantly limited by the fabrication of nanochannels, which is expensive, complicated, and often challenging during surface modification. However, in biochemical sensing applications, the device generally needs to be disposable because biochemical reactions are often irreversible or take a long time to reverse. To overcome the issues regarding the fabrication and surface modification of nanochannels, researchers proposed nanofluidic crystal as a facile and disposable nanofluidic biochemical sensor, benefitting from the low cost of nanoparticles and the ease of nanoparticle fabrication and modification. Utilizing the volume exclusion effect, Zharov and co-workers realized detection of cocaine in 100 nm and 290 nm nanofluidic crystals modified with cocaine-responsive aptamers. Upon the binding of cocaine, the immobilized aptamers changed to a

conformation with less space occupation, which increased the effective radius of the nanochannels and led to the increased ionic fluxes through the nanofluidic crystal.[57] Based on the electrostatic effect, Lei *et al.*[117] and Sang *et al.*[118] demonstrated nanofluidic crystal-based biochemical sensing of biotin and human α-thrombin in low ionic concentrations ($<10^{-5}$ M), achieving a similar LOD of ~1 nM. In the work of Sang *et al.*, upon the binding of human α-thrombin to the negatively charged aptamer-modified 540 nm nanofluidic crystal, the surface charge density of the nanoparticles increased, which led to the increase of the conductance of the nanofluidic crystal (Figure 11(a)). By further incubating an affinity aptamer with the human-α-thrombin-bound nanofluidic crystal, a sandwich structure of aptamer-thrombin-aptamer was formed, which displayed increased surface charge density and enhanced the conductance variation. One of the challenges of Sang's work in practical applications is that significant device-to-device variation exists due to the poor geometry controllability of self-assembled nanoparticles in micropores. To improve the readout consistency of nanofluidic crystal-based sensors, Zhao *et al.* designed a tunnel-shaped confined space for nanoparticle packing with an electrode pair beneath the nanoparticles, rather than the design in previous work where the electrode pair was placed at the two ends of nanofluidic crystal.[77] With the new design, the conductance of nanofluidic crystal measured through the electrode pair was dominated by nanoparticles inside the confined space, while irregularly packed nanoparticles outside the confined space had a negligible effect. The readout from different chips (n=16) had a coefficient of variation of 8.4%, which guaranteed self-calibration-free biochemical sensing.

Essentially, in order to realize highly sensitive biochemical detection in nanofluidic crystal, the key is to maximize the change of electrical conductance upon the binding of target molecules. For nanofluidic sensors based on the volume exclusion effect, one could use nanoparticles with interstices comparable to size of target biomolecules, and/or employ affinity probes with large conformation changes upon target recognition, which is a more effective approach for small molecules of interest. In the case of electrostatic effect-based sensors, this could be achieved by several strategies: first, using nanoparticles of smaller diameters could increase the ratio of surface conductance and bulk conductance, thereby making the device more surface charge-sensitive; lowering the ionic concentration could increase the Debye length and in turn increase the surface charge-sensitivity, but it is not always desirable and possible to use low ionic concentrations in handling real biochemical samples; one can also introduce a secondary highly charged probe after capturing the target molecules to increase the variation of surface charge density; last but not the least, decreasing the number of nanoparticles in the nanofluidic crystal could reduce the number of target molecules needed to be captured to elicit detectable changes in electrical conductance, thus potentially increasing the LOD.

The next hurdle for the practical applications of electrostatic effect-based sensing is that extremely diluted buffer is required to keep the nanofluidic crystal in the surface charge-governed regime. To circumvent this problem, the Wang group coupled nanofluidic crystal with Nafion-induced ion concentration polarization in a cross-shaped nanofilter chip, which temporarily created a low ion concentration zone and brought the nanofluidic crystal into the surface charge-sensitive regime (Figure 11(b)).[119] Samples in normal physiological conditions (biotin in 160 mM phosphate buffered saline (PBS) for proof-of-concept) was

introduced into the chip and incubated with surface-modified nanoparticles. Next, an ion depletion zone covering the nanofluidic crystal was formed by Nafion, immediately after which the conductance of the nanofluidic crystal was measured. It has been preliminarily demonstrated that the ion depletion effect can induce a temporarily low ionic concentration zone down to 10^{-4} M, which successfully enabled biotin detection in PBS.[119] The detection of biomolecules in clinical samples was further investigated with the nanofluidic crystal-ICP coupled strategy, which would potentially make it a truly enabling technique for rapid biochemical sensing at the point-of-care.[120]

5. Summary and perspectives

Nanofluidics has been an emerging researched field for the past 15 years, with over 20,000 papers indexed in Google Scholar. Up to date, the only material that enables nanofabrication-free, high-throughput, yet precisely controllable nanofluidics is the close-packed nanoparticle array, *i.e.* nanofluidic crystal, with significant potential in realizing point-of-care applications, high-power energy harvesting and various other applications. This review paper summarized the fundamental principles, models, current fabrication techniques and applications in various fields of nanofluidic crystal.

As reviewed, fundamentals and a broad variety of applications of nanofluidic crystal has been studied in the past 10 years. In the next several years, we can expect the following breakthroughs in nanofluidic crystal, which would have profound impacts on micro/nanofluidics and even broader areas:

1. Designable nanofluidic (crystal) device: Presently, nanofluidic devices are usually designed through a trial-and-error approach along with complicated full-scale numerical simulation, which is extremely time consuming and fails to design integrated nanofluidic devices with multiple functional units. With shared fundamental physics and governing equations in nanofluidics and semiconductors, bridging nanofluidics with the well-established microelectronics and therefore using the electronic design automation (EDA) softwares to design nanofluidic devices is promising. Interpreting nanofluidic crystal in a microelectronics way, as shown in section 3.3, has been pioneered recently and demonstrated feasibility in understanding complicated nanofluidic crystal devices. In the near future, it would be reasonable for us to have a fully designable nanofluidic crystal device, even with multiple functions integration, through the EDA tools. To reach this goal, deep understandings of ion transport in electrolytes and the semiconductor model of the electrolyte-electrode interface will be the first two key issues to address.
2. Ultrahigh sensitivity and label-free biochemical sensing: As most targets of interest exist in electrolytes and as charged molecules, nanofluidics, which handles ion transport and reflects surface charge property sensitively, is a perfect platform for sensitive biochemical sensing. Pushing the sensitivity to even higher is important for overcoming the challenges from terrorism threats, rapid mutation of virus or bacteria, cancer diagnostics and other circumstances where even detection of a single molecule is required. Benefiting from the progress in

designable nanofluidic device, an ultra high-sensitivity and label-free biochemical sensing may be realized by either achieving a single nanoparticle (singly doped) nanofluidic crystal device or *in-situ* integrating with a signal-amplification ionic circuit. To establish a nanofluidic crystal sensor with ultra-high sensitivity, designing devices that can precisely control single nanoparticles or with integrated multiple nanofluidic crystal functional units will be the first challenge to overcome.

3. Exploration of novel applications: With its ability of regulating the transport of ions/molecules/particles, we believe nanofluidic crystal also has unexplored potentials in drug delivery, micro-environment analysis of tumor cells, organ-on-a-chip, and many other fields. For example, nanofluidic diodes can be useful in controlled delivery of drugs and regulating the electrolyte environment of cells and tissues. Many nanofluidic energy conversion mechanisms, such as streaming potential, could also be transplanted to nanofluidic crystal for high power output applications.

4. Nano Total Analysis Systems (NanoTAS): Nanofluidic crystal brings nanofluidics closer to real-world applications, because of the higher throughputs that match practical needs. With nanofluidic crystal, various nanofluidic functional components, including power source (energy harvester), electrical valving (diodes and transistors), sample mixing (ICP mixer), molecular separation, sample analysis (sensors), and signal amplification (ICP preconcentrator), have been relatively well developed. It is reasonable to expect the integration of these components into self-contained Nano Total Analysis Systems (NanoTAS) in the future. To achieve this goal, efforts should be directed towards three directions: first, further improvement of the performances of nanofluidic components, such as the output power of energy harvesting, rectifying factor of nanofluidic diodes/transistors, and sensitivity of nanofluidic biosensors; second, advanced fabrication techniques should be developed, which can be largely learned from the photonic crystal community, to enable the development of more robust and complex nanofluidic devices/systems; lastly, solving the coupling issues of nanofluidic components is an important subject yet to be explored.

Supplementary Material

Refer to Web version on PubMed Central for supplementary material.

Acknowledgments

This work was financially supported by the Major State Basic Research Development Program (973 Program, Grant No. 2015CB352100), the National Natural Science Foundation of China (Grant No. 81471750 and 91323304), Beijing Natural Science Foundation (Grant No. 4172028), the Seeding Grant for Medicine and Information Sciences (2016-MI-04) of Peking University, and the MIT-Greater China MISTI program. J. Han and W. Ouyang were also supported by NIH (U19 AI109755).

References

1. Sparreboom W, Van Den Berg A, Eijkel JCT. Nat Nanotechnol. 2009; 4:713–720. [PubMed: 19898499]
2. Abgrall P, Nguyen NT. Anal Chem. 2008; 80:2326–2341. [PubMed: 18321133]
3. Bocquet L, Charlaix E. Chem Soc Rev. 2010; 39:1073–1095. [PubMed: 20179826]
4. Eijkel JCT, Van Den Berg A. Microfluid Nanofluid. 2005; 1:249–267.
5. Mijatovic D, Eijkel JCT, Van Den Berg A. Lab Chip. 2005; 5:492–500. [PubMed: 15856084]
6. Napoli M, Eijkel JCT, Pennathur S. Lab Chip. 2010; 10:957–985. [PubMed: 20358103]
7. Noy A, Park HG, Fornasiero F, Holt JK, Grigoropoulos CP, Bakajin O. Nano Today. 2007; 2:22–29.
8. Cheng LJ, Guo LJ. Chem Soc Rev. 2010; 39:923–938. [PubMed: 20179815]
9. Vlassiouk I, Siwy ZS. Nano Lett. 2007; 7:552–556. [PubMed: 17311462]
10. Vlassiouk I, Kozel TR, Siwy ZS. J Am Chem Soc. 2009; 131:8211–8220. [PubMed: 19507907]
11. Karnik R, Castelino K, Fan R, Yang P, Majumdar A. Nano Lett. 2005; 5:1638–1642. [PubMed: 16159198]
12. Liu Y, Yobas L. Nano Lett. 2014; 14:6983–6990. [PubMed: 25366228]
13. Duan C, Alibakhshi MA, Kim DK, Brown CM, Craik CS, Majumdar A. ACS Nano. 2016; 10:7476–7484. [PubMed: 27472431]
14. Daiguji H, Yang P, Szeri AJ, Majumdar A. Nano Lett. 2004; 4:2315–2321.
15. Van der Heyden FHJ, Bonthuis DJ, Stein D, Meyer C, Dekker C. Nano Lett. 2006; 6:2232–2237. [PubMed: 17034089]
16. Ren Y, Stein D. Nanotechnology. 2008; 19:195707. [PubMed: 21825725]
17. Kim DK, Duan C, Chen YF, Majumdar A. Microfluid Nanofluid. 2010; 9:1215–1224.
18. Tegenfeldt JO, Prinz C, Cao H, Huang RL, Austin RH, Chou SY, Cox EC, Sturm JC. Anal Bioanal Chem. 2004; 378:1678–1692. [PubMed: 15007591]
19. Piruska A, Gong M, Sweedler JV, Bohn PW. Chem Soc Rev. 2010; 39:1060–1072. [PubMed: 20179825]
20. van den Berg A, Wessling M. Nature. 2007; 445:726–726. [PubMed: 17301783]
21. Austin R. Nat Nanotechnol. 2007; 2:79–80. [PubMed: 18654220]
22. Wang S, Lee LJ. Biomicrofluidics. 2013; 7:011301.
23. Duan C, Wang W, Xie Q. Biomicrofluidics. 2013; 7:026501.
24. Karnik R, Castelino K, Duan C, Majumdar A. Nano Lett. 2006; 6:1735–1740. [PubMed: 16895365]
25. Xia Y, Gates B, Yin Y, Lu Y. Adv Mater. 2000; 12:693–713.
26. Norris DJ, Arlinghaus EG, Meng L, Heiny R, Scriven LE. Adv Mater. 2004; 16:1393–1399.
27. Ben-Moshe M, Alexeev VL, Asher SA. Anal Chem. 2006; 78:5149–5157. [PubMed: 16841941]
28. Mezzenga R, Ruokolainen J, Fredrickson GH, Kramer EJ, Moses D, Heeger AJ, Ikkala O. Science. 2003; 299:1872–1874. [PubMed: 12649476]
29. Zheng S, Ross E, Legg MA, Wirth MJ. J Am Chem Soc. 2006; 128:9016–9017. [PubMed: 16834358]
30. Zeng Y, Harrison DJ. Anal Chem. 2007; 79:2289–2295. [PubMed: 17302388]
31. Schoch RB, Han J, Renaud P. Rev Mod Phys. 2008; 80:839.
32. Chen Z, Wang Y, Wang W, Li Z. Appl Phys Lett. 2009; 95:102105.
33. Schoch RB, Van Lintel H, Renaud P. Phys Fluids. 2005; 17:100604.
34. Rubinstein I, Zaltzman B. Phys Rev E. 2000; 62:2238.
35. Pham VS, Li Z, Lim KM, White JK, Han J. Phys Rev E. 2012; 86:046310.
36. Jia M, Kim T. Anal Chem. 2014; 86:7360–7367. [PubMed: 25033014]
37. Tsukahara T, Mawatari K, Hibara A, Kitamori T. Anal Bioanal Chem. 2008; 391:2745–2752. [PubMed: 18581104]
38. Pronk S, Frenkel D. J Chem Phys. 1999; 110:4589–4592.

39. Reiss H. J Chem Phys. 1953; 21:1209–1217.
40. Vijh AK. J Mater Sci. 1975; 10:123–135.
41. Shockley W. Nobel lecture. 1956:344–374.
42. Cheng LJ. Ion and molecule transport in nanochannels, ProQuest. 2008
43. Shao L, Zheng M, Wang W. Appl Phys Lett. 2015; 106:093105.
44. Li F, Josephson DP, Stein A. Angew Chem, Int Ed. 2011; 50:360–388.
45. Shiu JY, Kuo CW, Chen P. J Am Chem Soc. 2004; 126:8096–8097. [PubMed: 15225033]
46. Hayward RC, Saville DA, Aksay IA. Nature. 2000; 404:56–59. [PubMed: 10716438]
47. Masuda Y, Itoh T, Koumoto K. Langmuir. 2005; 21:4478–4481. [PubMed: 16032863]
48. Zhang H, Wirth MJ. Anal Chem. 2005; 77:1237–1242. [PubMed: 15732902]
49. Zheng S, Zhang H, Ross E, Le TV, Wirth MJ. Anal Chem. 2007; 79:3867–3872. [PubMed: 17419588]
50. Newton MR, Bohaty AK, White HS, Zharov I. J Am Chem Soc. 2005; 127:7268–7269. [PubMed: 15898748]
51. Newton MR, Bohaty AK, Zhang Y, White HS, Zharov I. Langmuir. 2006; 22:4429–4432. [PubMed: 16618198]
52. Schepelina O, Zharov I. Langmuir. 2007; 23:12704–12709. [PubMed: 17975940]
53. Smith JJ, Zharov I. Langmuir. 2008; 24:2650–2654. [PubMed: 18275224]
54. Smith JJ, Abbaraju RR, Zharov I. J Mater Chem. 2008; 18:5335–5338.
55. Schepelina O, Zharov I. Langmuir. 2008; 24:14188–14194. [PubMed: 19053656]
56. Abelow AE, Zharov I. Soft Matter. 2009; 5:457–462.
57. Abelow AE, White RJ, Plaxco KW, Zharov I. Collect Czech Chem Commun. 2011; 76:683–694.
58. Ignacio-de Leon PAA, Zharov I. Chem Commun. 2011; 47:553–555.
59. Ignacio-de Leon PA, Abelow AE, Cichelli JA, Zhukov A, Stoikov II, Zharov I. Isr J Chem. 2014; 54:767–773.
60. Ouyang W, Wang W, Zhang H, Wu W, Li Z. Nanotechnology. 2013; 24:345401. [PubMed: 23899953]
61. Choi E, Kwon K, Kim D, Park J. Lab Chip. 2015; 15:168–178. [PubMed: 25328008]
62. Choi E, Kwon K, Kim D, Park J. Lab Chip. 2015; 15:512–523. [PubMed: 25407418]
63. Choi E, Kwon K, Lee SJ, Kim D, Park J. Lab Chip. 2015; 15:1794–1798. [PubMed: 25710479]
64. Choi E, Wang C, Chang GT, Park J. Nano Lett. 2016; 16:2189–2197. [PubMed: 26990504]
65. Jiang P, Bertone JF, Hwang KS, Colvin VL. Chem Mater. 1999; 11:2132–2140.
66. Dimitrov AS, Nagayama K. Langmuir. 1996; 12:1303–1311.
67. Zharov I, Khabibullin A. Acc Chem Res. 2014; 47:440–449. [PubMed: 24397245]
68. Wei B, Malkin DS, Wirth MJ. Anal Chem. 2010; 82:10216–10221. [PubMed: 21105703]
69. Wei B, Rogers BJ, Wirth MJ. J Am Chem Soc. 2012; 134:10780–10782. [PubMed: 22708746]
70. Rogers BJ, Wirth MJ. ACS Nano. 2012; 7:725–731. [PubMed: 23237590]
71. Zeng Y, He M, Harrison DJ. Angew Chem. 2008; 120:6488–6491.
72. Allain C, Limat L. Phys Rev Lett. 1995; 74:2981. [PubMed: 10058073]
73. Lee WP, Routh AF. Langmuir. 2004; 20:9885–9888. [PubMed: 15518466]
74. Dufresne ER, Corwin EI, Greenblatt NA, Ashmore J, Wang DY, Dinsmore AD, Cheng JX, Xie XS, Hutchinson JW, Weitz DA. Phys Rev Lett. 2003; 91:224501. [PubMed: 14683242]
75. Kanai T, Sawada T. Langmuir. 2009; 25:13315–13317. [PubMed: 19874037]
76. Wang L, Zhao XS. J Phys Chem C. 2007; 111:8538–8542.
77. Zhao W, Wang B, Wang W. Lab Chip. 2016; 16:2050–2058. [PubMed: 27098158]
78. Guo W, Tian Y, Jiang L. Acc Chem Res. 2013; 46:2834–2846. [PubMed: 23713693]
79. Ai Y, Liu J, Zhang B, Qian S. Sens Actuator B-Chem. 2011; 157:742–751.
80. Cao L, Guo W, Wang Y, Jiang L. Langmuir. 2011; 28:2194–2199. [PubMed: 22148901]
81. Kong Y, Fan X, Zhang M, Hou X, Liu Z, Zhai J, Jiang L. ACS Appl Mater Interfaces. 2013; 5:7931–7936. [PubMed: 23844847]

82. Vilozny B, Wollenberg AL, Actis P, Hwang D, Singaram B, Pourmand N. Nanoscale. 2013; 5:9214–9221. [PubMed: 23934399]
83. Yeh LH, Hughes C, Zeng Z, Qian S. Anal Chem. 2014; 86:2681–2686. [PubMed: 24484296]
84. Lei Y, Wang W, Wu W, Li Z. Appl Phys Lett. 2010; 96:263102.
85. Rao S, Si KJ, Yap LW, Xiang Y, Cheng W. ACS Nano. 2015; 9:11218–11224. [PubMed: 26486960]
86. Choi E, Wang C, Chang GT, Park J. Nano Letters. 2016
87. Pu Q, Yun J, Temkin H, Liu S. Nano Lett. 2004; 4:1099–1103.
88. Wang YC, Stevens AL, Han J. Anal Chem. 2005; 77:4293–4299. [PubMed: 16013838]
89. Kim SJ, Song YA, Han J. Chem Soc Rev. 2010; 39:912–922. [PubMed: 20179814]
90. Kim SJ, Ko SH, Kang KH, Han J. Nat Nanotechnol. 2010; 5:297–301. [PubMed: 20305644]
91. Lee SJ, Kim D. Microfluid Nanofluid. 2012; 12:897–906.
92. Kim M, Jia M, Kim T. Analyst. 2013; 138:1370–1378. [PubMed: 23293785]
93. Choi, E., Kwon, K., Lee, SJ., Kim, D., Park, J. IEEE MEMS 2012. Paris, France: 2012.
94. Syed A, Mangano L, Mao P, Han J, Song YA. Lab Chip. 2014; 14:4455–4460. [PubMed: 25254651]
95. Pattle RE. Nature. 1954; 174:660–660.
96. Guo W, Cao L, Xia J, Nie FQ, Ma W, Xue J, Song Y, Zhu D, Wang Y, Jiang L. Adv Funct Mater. 2010; 20:1339–1344.
97. Wang ZL. Sci Am. 2008; 298:82–87.
98. Yao S, Anex DS, Caldwell WB, Arnold DW, Smith KB, Schultz PG. Proc Natl Acad Sci U S A. 1999; 96:5372–5377. [PubMed: 10318890]
99. Herr AE, Singh AK. Anal Chem. 2004; 76:4727–4733. [PubMed: 15307783]
100. Volkmuth WD, Austin RH. Nature. 1992; 358:600–602. [PubMed: 1501715]
101. Han J, Craighead HG. Science. 2000; 288:1026–1029. [PubMed: 10807568]
102. Chou CF, Bakajin O, Turner SWP, Duke TAJ, Chan SS, Cox EC, Craighead HG, Austin RH. Proc Natl Acad Sci U S A. 1999; 96:13762–13765. [PubMed: 10570146]
103. Huang LR, Tegenfeldt JO, Kraeft JJ, Sturm JC, Austin RH, Cox EC. Nat Biotechnol. 2002; 20:1048–1051. [PubMed: 12219075]
104. Huang LR, Cox EC, Austin RH, Sturm JC. Science. 2004; 304:987–990. [PubMed: 15143275]
105. Han J, Turner SW, Craighead HG. Phys Rev Lett. 1999; 83:1688.
106. Turner SWP, Cabodi M, Craighead HG. Phys Rev Lett. 2002; 88:128103. [PubMed: 11909505]
107. Van Oudenaarden A, Boxer SG. Science. 1999; 285:1046–1048. [PubMed: 10446046]
108. Yamada M, Nakashima M, Seki M. Anal Chem. 2004; 76:5465–5471. [PubMed: 15362908]
109. Meistermann L, Tinland B. Phys Rev E. 2000; 62:4014.
110. Birdsall RE, Koshel BM, Hua Y, Ratnayaka SN, Wirth MJ. Electrophoresis. 2013; 34:753–760. [PubMed: 23229163]
111. Zeng Y, He M, Harrison DJ. Angew Chem, Int Ed. 2008; 47:6388–6391.
112. Nazemifard N, Bhattacharjee S, Masliyah JH, Harrison DJ. Angew Chem, Int Ed. 2010; 49:3326–3329.
113. Ye, W., Wang, L., Nazemifard, N., Harrison, DJ. presented in part at the MicroTAS 2010; Groningen, The Netherlands. 2010.
114. Nazemifard N, Wang L, Ye W, Bhattacharjee S, Masliyah JH, Harrison DJ. Lab Chip. 2012; 12:146–152. [PubMed: 22105746]
115. Ali M, Yameen B, Neumann R, Ensinger W, Knoll W, Azzaroni O. J Am Chem Soc. 2008; 130:16351–16357. [PubMed: 19006302]
116. Schoch RB, Cheow LF, Han J. Nano Lett. 2007; 7:3895–3900. [PubMed: 17997589]
117. Lei Y, Xie F, Wang W, Wu W, Li Z. Lab Chip. 2010; 10:2338–2340. [PubMed: 20544114]
118. Sang J, Du H, Wang W, Chu M, Wang Y, Li H, Zhang HA, Wu W, Li Z. Biomicrofluidics. 2013; 7:024112.

119. Ouyang, W., Sang, J., Shi, Y., Wang, W., Chu, M., Wang, Y., Li, H., Zhang, H., Wu, W., Li, Z. presented in part at the MicroTAS 2013; Freiburg, Germany. 2013.

120. Ouyang W, Han J, Wang W. Enabling Electrical Biomolecular Detection in High Ionic Concentrations and Signal Enhancement Thereof by Coupling Nanofluidic Crystal with Reconfigurable Ion Concentration Polarization, under review. 2017

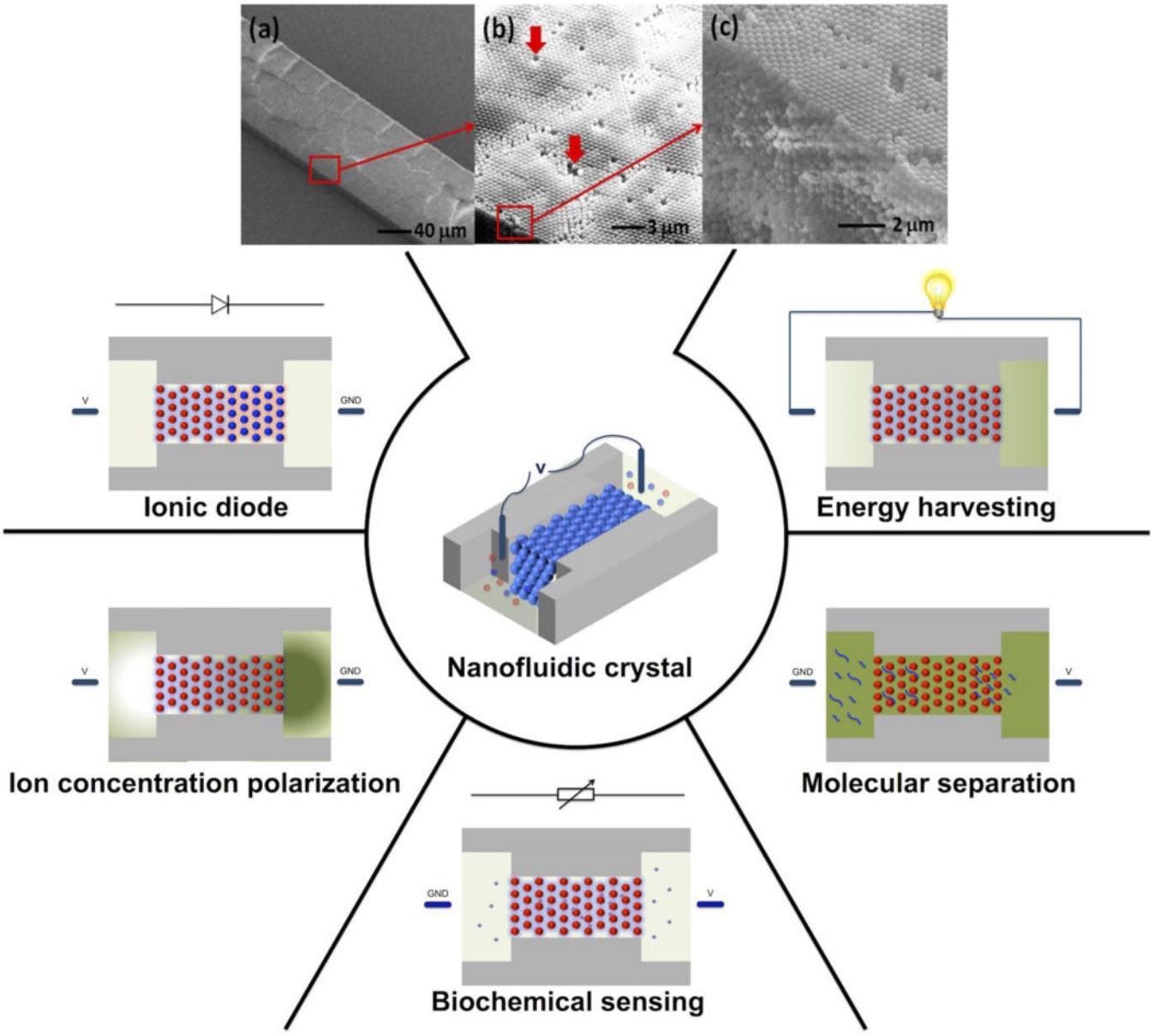

Figure 1.

Schematic diagram of nanofluidic crystal in various applications. The SEM images of nanofluidic crystal were adapted from ref.[32] with permission, copyright 2009, American Institute of Physics.

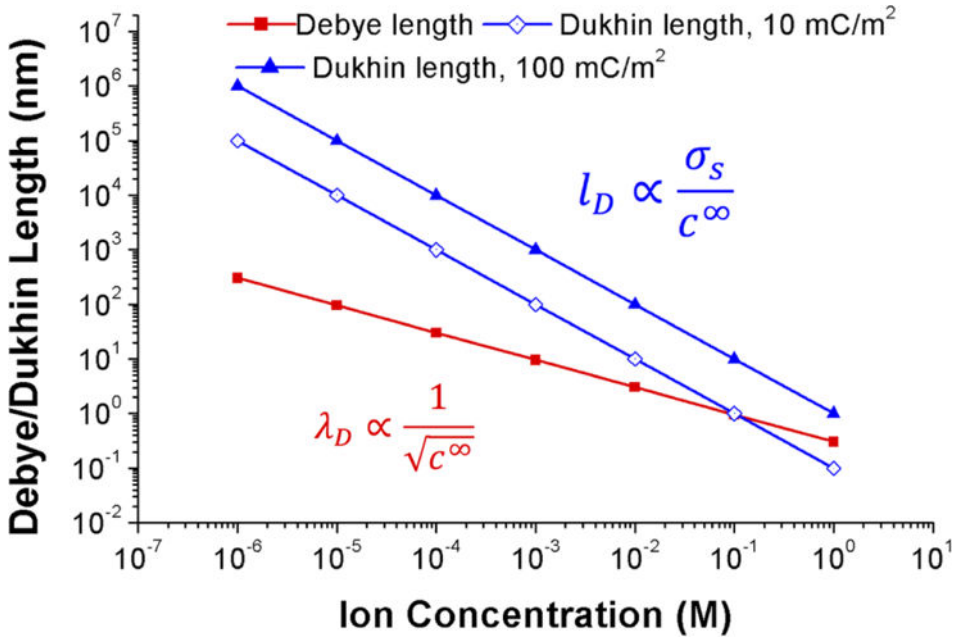

Figure 2.
Debye length and Dukhin length in different concentrations of KCl solutions.

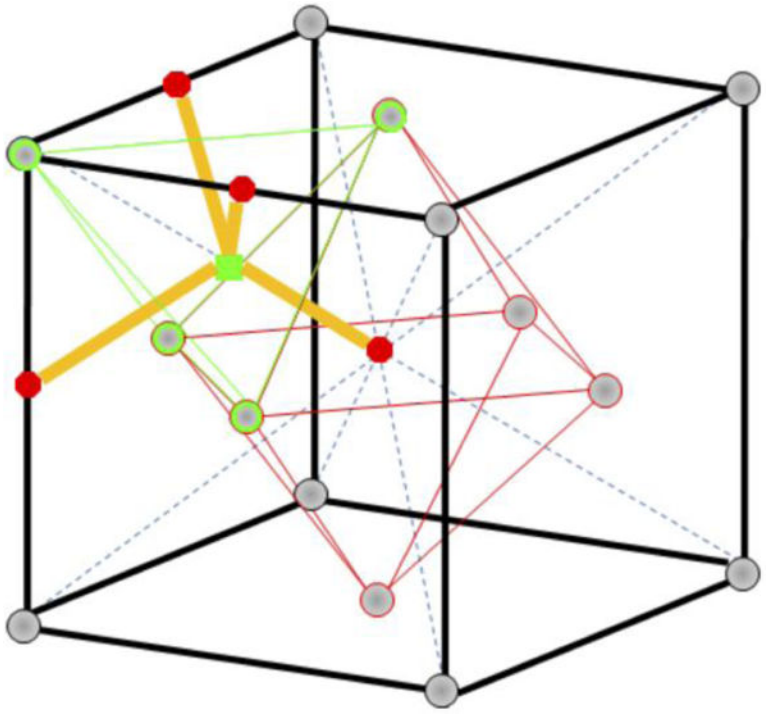

Figure 3.

The fcc lattice showing the tetrahedron interstitials (green square) and octahedron interstitials (red circle). Grey solid circles represent the centers of nanoparticles. Reproduced from ref.[32] with permission, copyright 2009, American Institute of Physics.

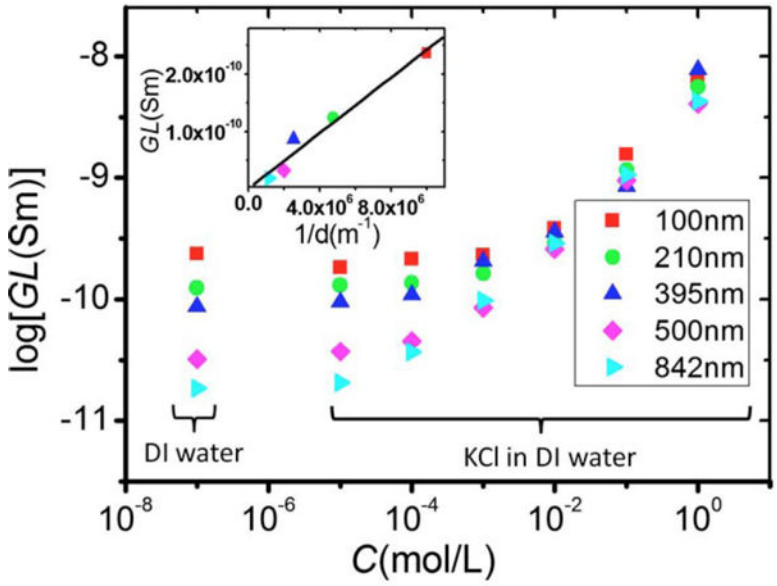

Figure 4.

Conductance of nanofluidic crystals packed with nanoparticles of different diameters at different KCl concentrations. Reproduced from ref.[32] with permission, copyright 2009, American Institute of Physics.

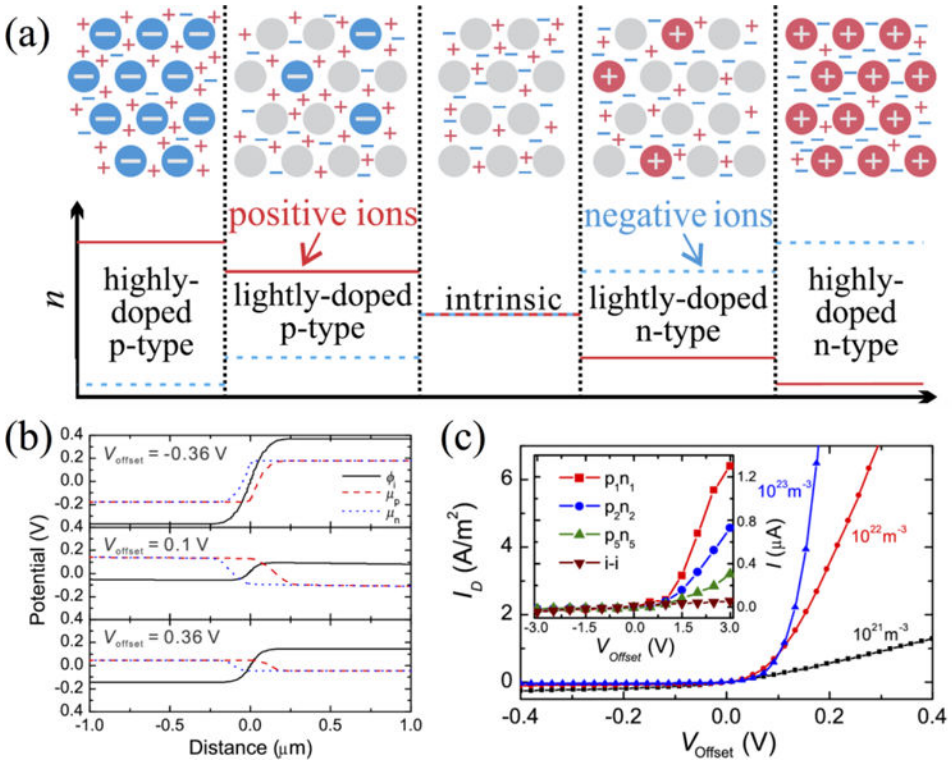

Figure 5.

(a) Schematic diagram of the nanoparticle doping concept. (b) Simulated electrostatic potential, electrochemical potential for hydrogen, and hydroxyl ions at different biases. (c) Simulated and experimental (inset) I-V curves of nanofluidic crystal diodes. Figures are adapted from ref.[43] with permission, copyright 2015, American Institute of Physics.

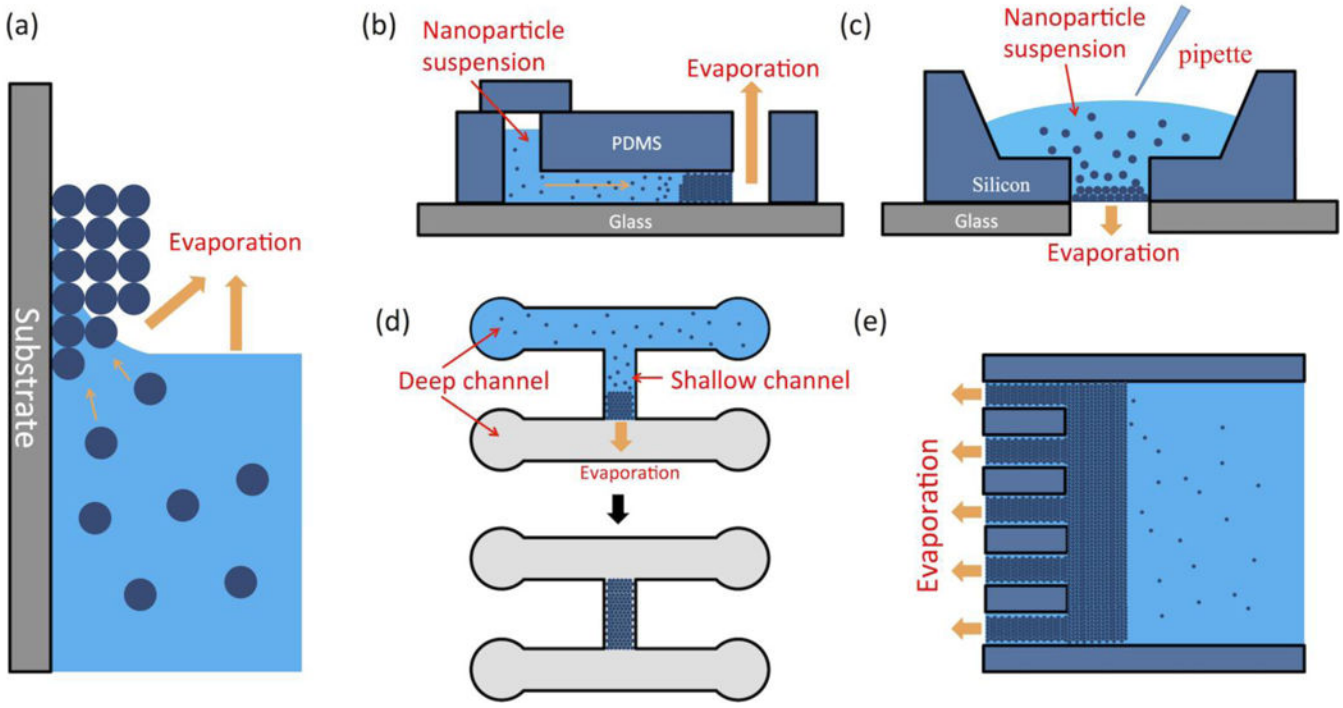

Figure 6.

Capillary force-assisted fabrication of nanofluidic crystal by (a) vertical deposition and (b–e) horizontal deposition. (b) Horizontal deposition in a single microchannel. (c) Horizontal deposition in a micropore. (d) Horizontal deposition in a specific region of a microfluidic chip. (e) Multi-channel guided crack-free large-area nanofluidic crystal.

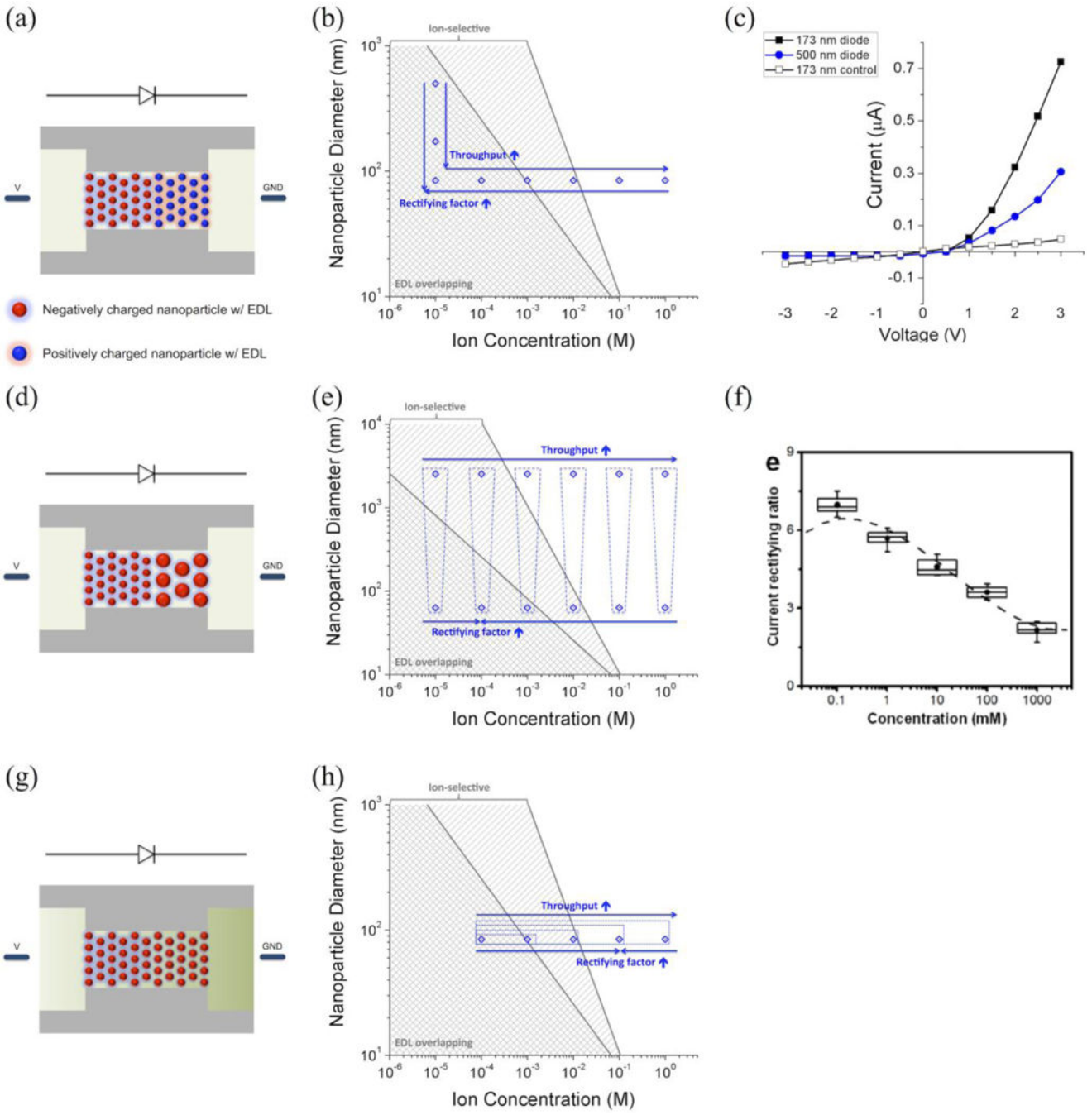

Figure 7.

Different types of nanofluidic crystal based diodes. A surface charge density of 25 mC/m^2 is used to calculate the Dukhin length and determine the ion-selective regime. (a) First type: diode based on the opposite charge polarities of nanoparticles. (b) Optimization of the first type of diode. (c) Experimental demonstration by Lei *et al.*[84] Experimental data were replotted from ref.[84] with original authors' permission. (d) Second type: diode based on nanoparticles of different diameters. (e) Optimization of the second type of diode. (f) Experimental demonstration by Rao *et al.*[85] Reproduced from ref.[85] with permission,

copyright 2015, American Chemical Society. (g) Third type: diode based on asymmetric bath concentrations. (h) Optimization of the third type of diode.

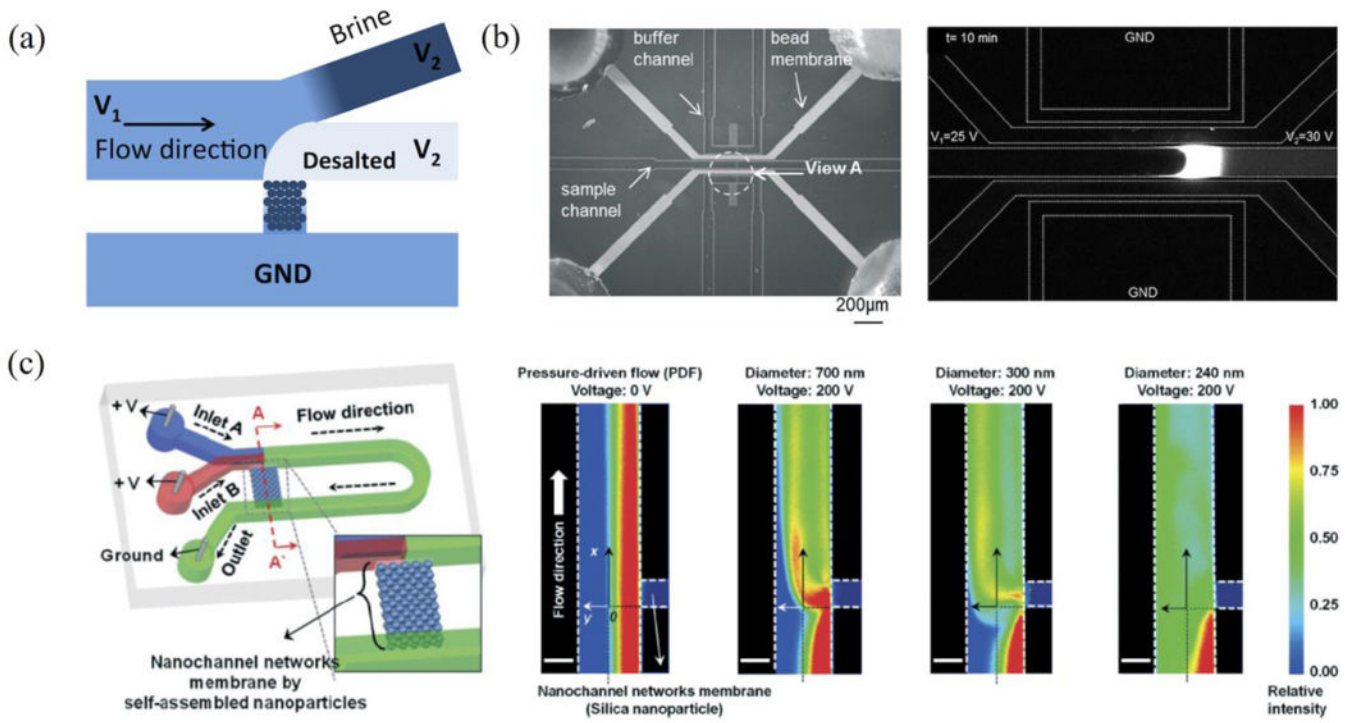

Figure 8.

Ion concentration polarization related applications of nanofluidic crystal. (a) Water desalination. (b) Biomolecule concentration. Reproduced from ref.[94] with permission, copyright 2014, Royal Society of Chemistry. (c) Chemical mixing. Reproduced from ref.[63] with permission, copyright 2015, Royal Society of Chemistry.

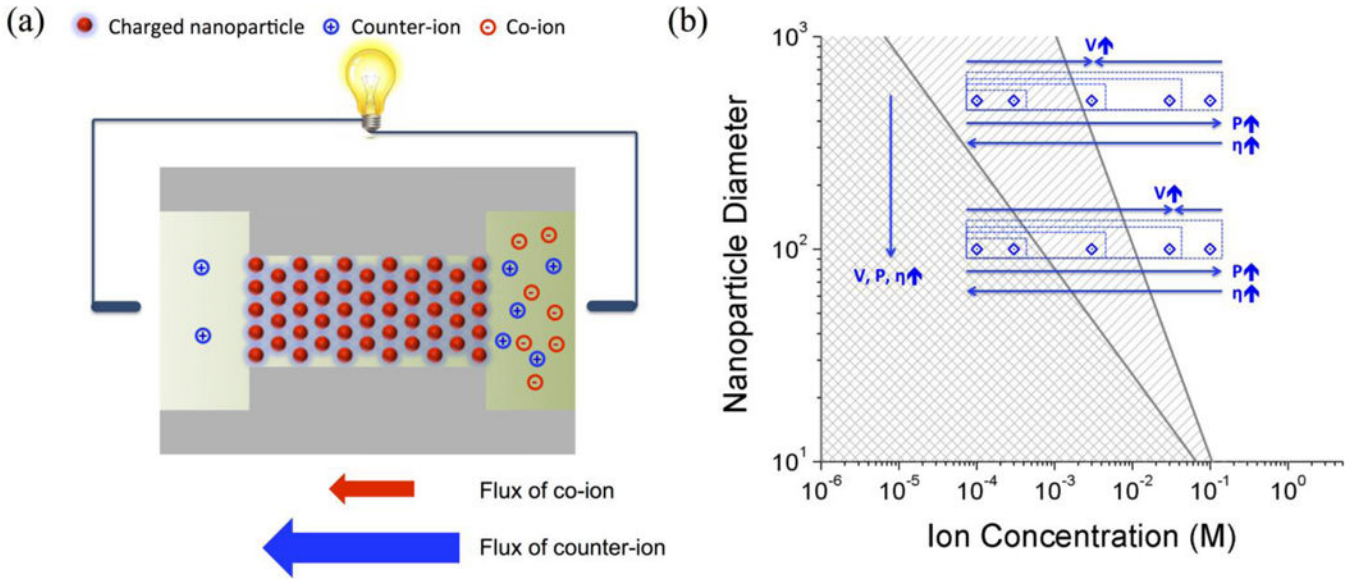

Figure 9.

(a) Schematic diagram of nanofluidic crystal-based energy harvesting by reverse electrodialysis. (b) Optimization of the energy harvesting performance. The chart was drawn according to the data in Ouyang *et al.*[60]

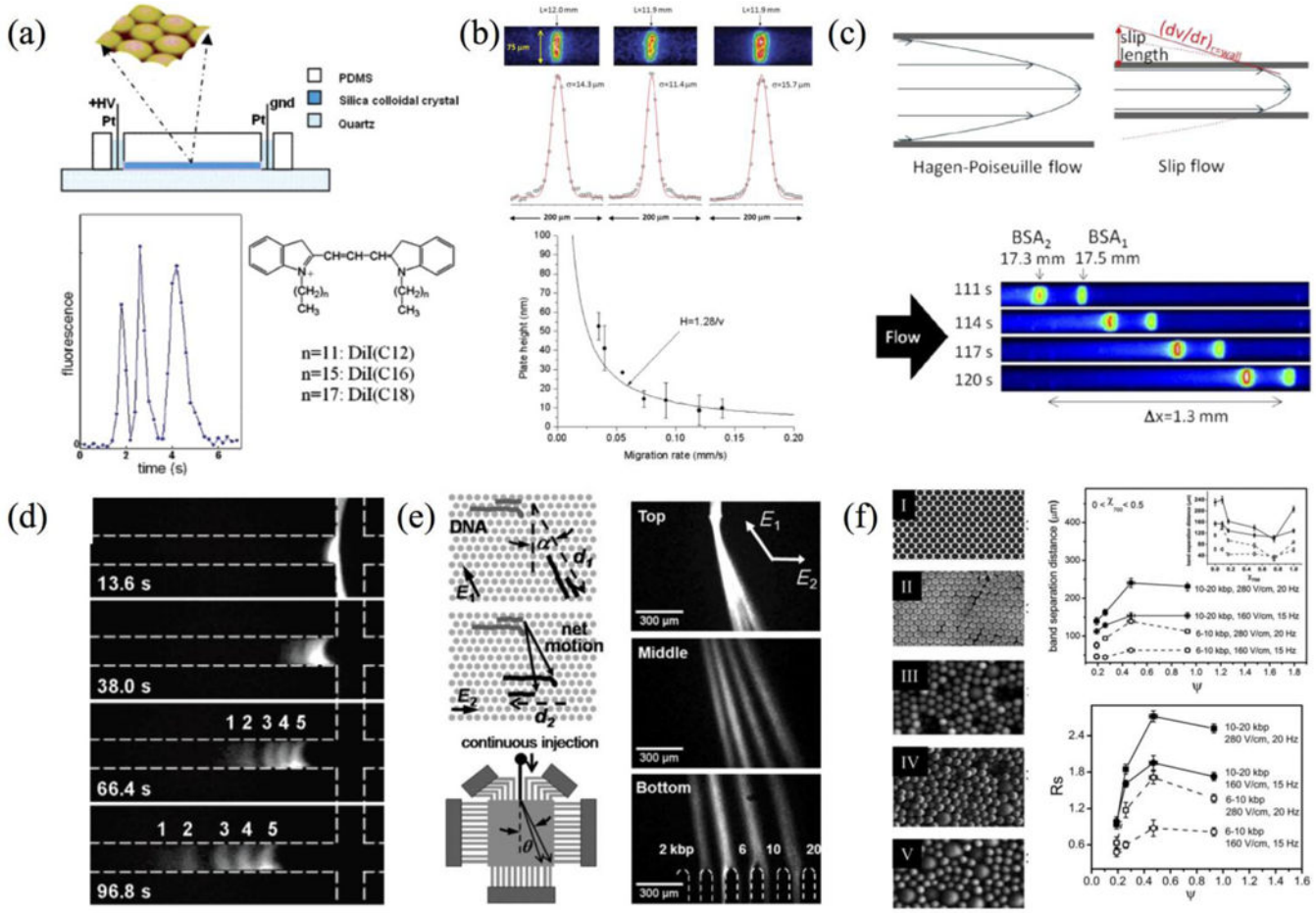

Figure 10.

Molecular separation in nanofluidic crystal. (a) Separation of structurally similar dyes. Reproduced from ref.[29] with permission, copyright 2006, American Chemical Society. (b) Sub-50 nm plate heights were achieved in nanofluidic crystal. Reproduced from ref.[68] with permission, copyright 2010, American Chemical Society. (c) BSA separation enhanced by slip flow in nanofluidic crystal. Reproduced from ref.[69] with permission, copyright 2012, American Chemical Society. (d) Fluorescence images of dsDNA separation. Reproduced from ref.[30] with permission, copyright 2007, American Chemical Society. (e) Continuous-flow separation of DNAs. Reproduced from ref.[111] with permission, copyright 2008, John Wiley and Sons. (f) Effect of degree of order on the performance of DNA separation in nanofluidic crystal. Reproduced from ref.[114] with permission, copyright 2012, Royal Society of Chemistry.

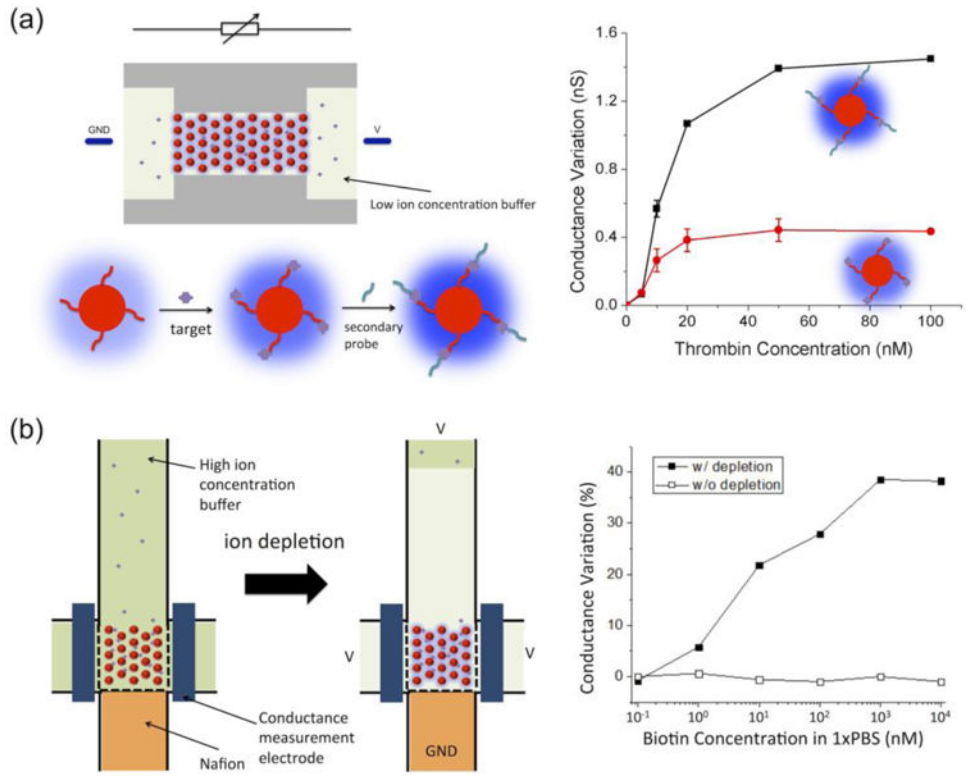

Figure 11.

(a) Biomolecular sensing in nanoparticle crystal at low ionic concentrations. Experimental data were replotted from ref.[118] with original authors' permission. (b) Biochemical sensing in physiological conditions enabled by coupling nanofluidic crystal with the ion depletion effect of ICP. Experimental data were replotted from ref.[119] with original authors' permission.

Table 1

Comparison of the features of different fabrication methods.

Method	Vertical deposition	Horizontal deposition			
Substrate/Device	Surface of glass, silicon, and other solid substrates	Single microchannel	Micropore	Specific region in a microfluidic chip	Large-area microfluidic chip
Characteristics	Substrate is open (not forming enclosed structures)	Usually long (>1 mm)	Forms thin membrane of nanoparticles	Needs assisting channels to deliver nanoparticles	Uses multiple guiding channels to avoid cracks
Ability to control morphology	Thickness precisely controllable, width and length determined by substrate	Morphology defined by device structure, but length of channel may vary	Morphology defined by device structure, but thickness of membrane may vary	Morphology defined by device structure	Morphology defined by device structure
Reproducibility	Good (crack avoidable, morphology controllable)	Moderate (crack avoidable, length of channel may vary)	Moderate (crack avoidable, thickness of membrane may vary)	Good (crack avoidable, morphology controllable)	Good (crack avoidable, morphology controllable)
Ability to scale up	Yes	No (crack formation in large area)	No (crack formation in large area, mechanical stability)	No (crack formation in large area)	Yes
Time	Days	Hours			
Cost	Low	Low	Depending on the cost of micropore fabrication	Low	Low